Title
THE SCATTERING AND ABSORPTION OF POSITIVE PI MESONS BY ALUMINUM

Author
Tracy, James Frueh.

Publication Date
1952-11-16

UCRL-2013
Unclassified-Physics Distribution

UNCLASSIFIED

UNIVERSITY OF CALIFORNIA

Radiation Laboratory

Contract No. W-7405-eng-48

THE SCATTERING AND ABSORPTION OF POSITIVE PI MESONS BY ALUMINUM

James Frueh Tracy

(Thesis)

November 16, 1952

Berkeley, California

DISCLAIMER

TABLE OF CONTENTS

TABLES AND FIGURES

THE SCATTERING AND ABSORPTION OF POSITIVE PI MESONS BY ALUMINUM

James Frueh Tracy

(Thesis)

Radiation Laboratory, Department of Physics
University of California, Berkeley, California

November 16, 1952

ABSTRACT

The interaction of π^+ mesons with aluminum has been studied by using a cloud chamber containing five 1/8-inch aluminum plates in a 5200-gauss field. Meson energies ranged from 25 to 100 Mev (average, 49 Mev). μ^+ contamination was 13 percent. Positron contamination was negligible. 20 stops, 34 scatters $\geqslant 30^\circ$, and 57 stars were observed. All stops are reasonably accounted for by scatters and stars hidden by the geometry. One event interpreted as an inelastic charge exchange scatter was observed. It consisted of a 1-prong star and a 70 Mev electron-positron pair in coincidence. The cross sections rise steeply with energy. The scattering (elastic plus inelastic) is very roughly isotropic except for a dip in the 60° to 90° interval and possibly for one in the 120° to 150° interval. Corrected absolute cross sections for the 25-45, 45-70, and 70-100 Mev intervals, respectively, are: σ(scat), 70 ± 23, 312 ± 74, and 216 ± 82 mb; σ(star), 176 ± 37, 299 ± 62, and 332 ± 100 mb; and σ(total), 246 ± 43, 611 ± 95, and 548 ± 129 mb. Detailed results, with a discussion of errors and a description of experimental apparatus and procedures, are given.

THE SCATTERING AND ABSORPTION OF POSITIVE PI MESONS BY ALUMINUM

James Frueh Tracy

(Thesis)

Radiation Laboratory, Department of Physics
University of California, Berkeley, California

November 16, 1952

INTRODUCTION

At the present time, the outstanding problem of nuclear physics is understanding the nature of nuclear forces. In 1935 Yukawa[1] postulated the existence of a new unstable particle as the basis for an exchange force between nucleons. In analogy with electromagnetic theory, each nucleon is considered to have an associated "meson field." The new particles (mesons) are the quanta of this field. The short-range character of nuclear forces requires that the meson have a finite rest mass. Yukawa predicted its mass to be intermediate between the electron and proton masses. In order to satisfy conservation of charge, these mesons would be required to carry positive or negative electronic charges.

Two years later, it became clear that just such an intermediate-mass particle existed in the penetrating component of cosmic radiation.[2, 3] It was at first identified with the Yukawa particle but, during the following decade, it became increasingly apparent that distressing discrepancies existed between the theoretical predictions concerning some of its properties, and the experimental facts. The experimentally observed lifetime of this particle - subsequently termed the mu (μ) meson, or muon - was much too long; its absorption by nuclear matter was much too weak, particularly since the inverse process of production appeared to proceed so strongly in cosmic radiation.

These difficulties were resolved in 1947 by the discovery of a more primitive particle - the pi (π) meson, or pion.[4, 5] The discovery of the π-μ decay sequence established the genetic relationship between pion and muon. It was thus the pion that was

produced in such abundance in the cosmic ray events of the upper atmosphere; the muon observed in the penetrating component of cosmic radiation was merely a secondary product, and resulted from the rapid decay of the pion.

The artificial production of mesons in 1948, at Berkeley[6] and their identification with the cosmic-ray pi mesons opened the way to a more controlled and intensive experimentation into the field of meson physics. Attention has since centered primarily upon the pion. Early work mainly concerned the processes by which mesons were produced. An experimental understanding of their production made it feasible to obtain mesons in collimated beams that could be used for scattering and absorption experiments.

To be specific with regard to the present experiment, by 1950 Richman, Wilcox, and co-workers[7] had produced a relatively high intensity, 54 Mev beam of π^+ mesons in the external 340 Mev proton beam of the 184-inch Berkeley cyclotron. It appeared practicable to bring these mesons outside the cyclotron radiation shielding and into a magnet cloud chamber, where their scattering and absorption by nuclear matter could be studied. The meson flux and the estimated interaction cross sections appeared such that a significant number of events could only be produced in a solid target, however. One would have preferred to undertake the more fundamental problem of investigating the interaction of mesons with protons or deuterons, but these simple nuclei are not available in solid form in the pure state, and would necessarily have to be introduced into a cloud chamber in the form of gaseous hydrogen or deuterium, which would have reduced the data rate by a factor of 1000.

The choice of aluminum as a target material was made somewhat arbitrarily. It was desired to use a fairly light (low Z) nucleus in order to minimize coulomb scattering. Aluminum satisfied this requirement and is also a solid, readily available and convenient to handle. From the practical standpoint, too,

aluminum is a material frequently employed in experimental equipment for thin windows, collimators, absorbers, as a structural material, etc.; whose cross-sectional data would be useful design information.

It was first planned to perform this experiment with a (continuous) diffusion cloud chamber[8-11] because it was expected that the data rate could be greatly increased over that obtainable with a conventional (expansion) chamber. Because of the difficulties encountered and the pressure of time the work was eventually performed with the conventional chamber.

It should be pointed out that many other experimenters have also been studying meson interactions. There is now a considerable amount of data on both interactions with nucleons, and interactions with complex nuclei. Much more data is still needed, of course, to fill in and extend the broad outlines of current knowledge. Reference to some of the published results will be made later under "Discussion".

RESULTS

The results obtained for the interaction of positive pi mesons with aluminum are presented graphically in Figures 1 and 2, and numerically, in somewhat more detail, in Tables I, II, and III. Additional information is presented below.

It is apparent that the absolute scattering, star, and total cross sections (Fig. 1 and Table I) have a rapid rise with energy and that the total cross section equals the nuclear area $[= (rA)^{2/3}$ $\approx$550 millibarns, $r \approx 1.4 \times 10^{-13}$ cm$]$ in the 60 Mev region and drops to half this value near 30 Mev. It is not clear whether it continues to rise, levels off, or eventually drops down again beyond 60 Mev. The star production cross section is about 50 percent greater than the scattering cross section.

Within the statistics, it appears possible to characterize the nuclear scattering as isotropic, although there is definite indication of a minimum between 60° and 90° and the possibility

of a second minimum between 120° and 150° (see Fig. 2) The differential scattering cross section, averaged over all energies and all angles $\geq 30^{\circ}$, is 12.9 ± 2.2 millibarns (Table II). The small angle scattering appears to follow the theoretical single coulomb scattering predictions reasonably well. The data are too course to draw conclusions about the interference between coulomb and nuclear scattering.

The data presented in this paper refer to the laboratory system. For all practical purposes - and far within the experimental uncertainties - this is, however, the same as referring the data to the center-of-mass system; the mass of the aluminum nucleus is 180 times the meson mass and the c.m. velocity is, for example, less than 1/200 that of the colliding meson when the latter has an energy of, say, 50 Mev.

In Table I, stars are listed as either 1-prong or 2-prong. Among the stars listed as 2-prong there are included one that actually had three prongs and another one that had four prongs. It is presumed that many of the stars emitted more than two ionizing fragments, but, that these additional fragments were too slow to escape the aluminum plates. Of the 83 star prongs that were observed, 49 were "fast" and 34 were "slow". The great majority of prongs appeared to be protons; for purposes of estimating prong energies, all were assumed to be protons. Fast protons were those estimated to have energies >30 Mev and slow prongs were those estimated to have energies <30 Mev. The angular distribution of the fast prongs was isotropic; their forward to backward ratio being 24:25. The slow prongs, on the other hand, were predominantly forward; their forward to backward ratio being 25:9.

It is of interest to note the number of 2-prong stars whose prongs were in approximately opposite directions. Altogether, there were five stars in which the prongs were opposite to within 30°. In three cases, where both prongs were fast, the included angle between the two prongs differed from

180° by 16°, 28°, and 30°, respectively. In two other stars, with one fast prong and one slow prong, the included angle differed from 180° by 16° and 29° respectively. For the first case (two fast prongs and 16°) the geometrical weight was 1/6.5, i.e., 5.5 similar events were probably hidden by the geometry. (See Appendix III for an explanation of the meaning of geometrical weight.) In the other four cases the geometrical weight was unity. The first case is shown in Fig. 19.

Of the many events photographed in the chamber, only one was strikingly unusual. It is shown in Fig. 14. An 88 Mev pion entered the third plate and a proton of approximately 51 Mev was ejected nearly straight forward ($\theta = 6^\circ$). In coincidence with this "1-prong star" there is a 70 Mev electron-positron pair. That this was an accidental coincidence is highly improbable. This event is interpreted as an inelastic charge-exchange scattering; the decay of the neutral pion gave rise to the electron pair. This event is analyzed more fully under "Discussion - The Unusual Event".

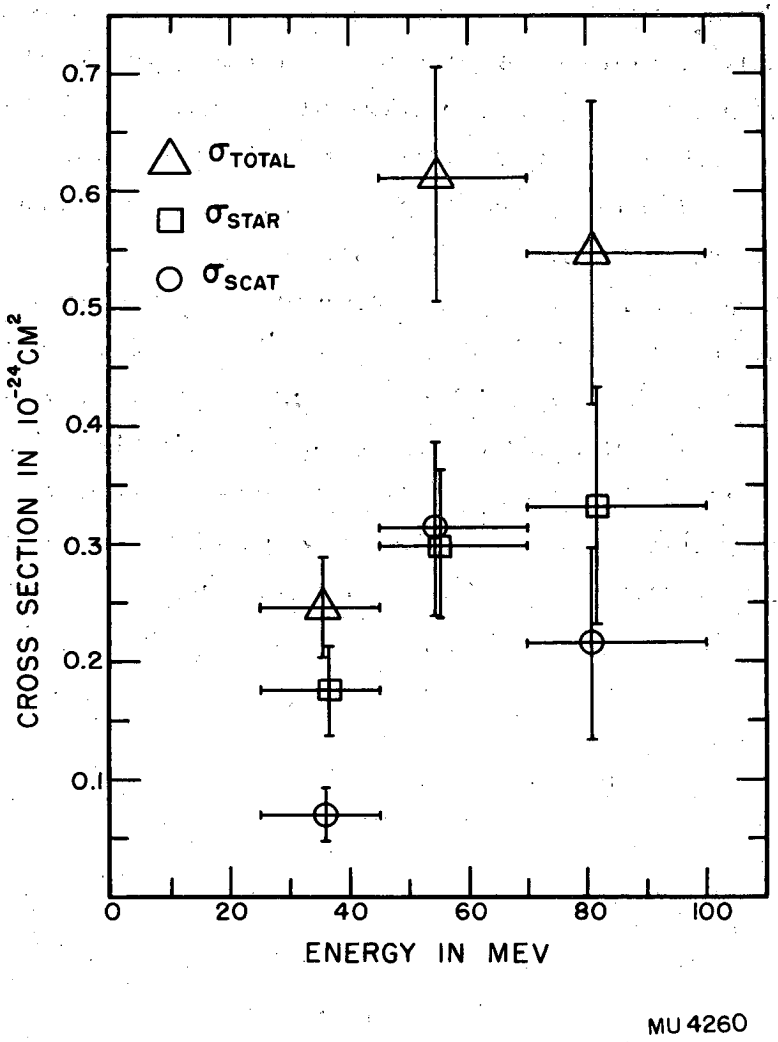

Fig. 1. - Absolute Cross Sections for the Interaction of Positive Pions with Aluminum

The data are based upon 111 events, which included scatters $\geqslant 30^{\circ}$, stars and stops. The stops have been apportioned between the scatters and stars in accordance with calculated geometrical corrections. The scattering cross sections have been extended to include the angles from 0° to 30° by using the average differential cross section between 30° and 180° to obtain a total scattering cross section over 4π steradians. No distinction between elastic and inelastic scattering events has been attempted. Standard deviations, based upon statistics only, and energy groupings are indicated for the abscissae and ordinates, respectively. ($\bar{\sigma}_{total} \doteq \bar{\sigma}_{star} + \bar{\sigma}_{scat}$).

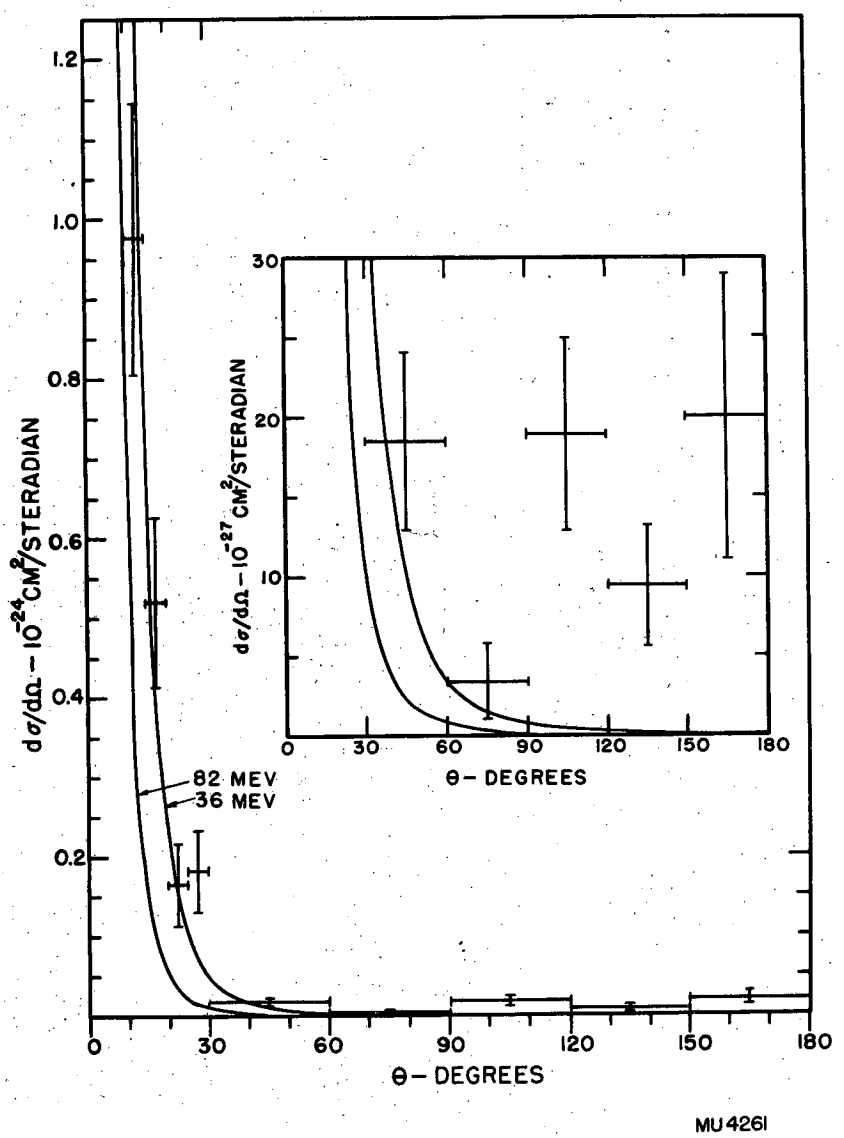

Fig. 2. Differential Cross Sections for Scattering of Positive Pions by Aluminum

The plotted points are experimental values based upon 114 scatters between 10° and 180° (34, between 30° and 180°) of pions having energies between 25 and 100 Mev (mean energy = 49 Mev). Standard deviations based upon statistics, and angular groupings are indicated. The solid curves represent theoretical single coulomb scattering at two different energies for comparison purposes. The inset reproduces a portion of the same data to an enlarged ordinate scale.

Table I. - Data on the Interaction of 25-100 Mev Positive Pions with Aluminum

Energy Interval (Mev)	Observed Number of Events: Stops	Scatters $\geq 30^{o}$	1-prong stars	2-prong stars	Corrected Number of Events: Scatters $\geq 30^{o}$	1-prong stars	2-prong stars	Absolute Cross Sections (corrected for geometry and mu contamination) (millibarns): Scattering	Star production	Total
	n^0	n^S	n^1	n^2	N^S	N^1	N^2	σ_{scat}	σ_{star}	σ_{total}
25-45	9	9	18	5	10.6	14.2	14.5	70±23	176±37	246±43
45-70	8	18	10	13	25.1	8.2	17.3	312±74	299±62	611±95
70-100	3	7	6	5	7.9	6.8	6.2	216±82	332±100	548±129
(Total) 25-100	20	34	34	23	43.6	29.2	38.0	162±28	234±31	396±41

The definition of symbols is given in Appendix IV. Elastic and inelastic scatters have not been separated. The absolute cross sections have been corrected for events hidden by geometry and for the error in the pion count introduced by the muon contamination. The absolute scattering cross sections have been computed by extending the average differential cross section for scatters $\geq 30^{o}$ over the total solid angle of 4 π steradians. The indicated uncertainties are standard deviations based upon numbers of events only. Most of these cross sections are presented graphically in Fig. 1.

Table II. - Data on the Scattering of 25-100 Mev Positive Pions by Aluminum

Energy Interval (Mev)	Scattering Angle - θ (Angular interval in degrees) 10-15	15-20	20-25	25-30	30-60	60-90	90-120	120-150	150-180	30-180
	Number of scatters actually observed									
25-45	24	16	8	7	3	1	2	1	2	9
45-70	8	6	2	3	5	0	7	4	2	18
70-100	1	2	0	3	3	1	1	1	1	7
(Total) 25-100	33	24	10	13	11	2	10	6	5	34
	Number of scatters after correction for those hidden by geometry									
25-45	24.0	16.0	8.0	7.0	3.1	1.5	3.0	1.0	2.0	10.6
45-70	8.0	6.0	2.0	3.0	5.9	0.0	12.9	4.3	2.0	25.1
70-100	1.0	2.0	0.0	3.0	3.1	1.6	1.2	1.0	1.0	7.9
(Total) 25-100	33.0	24.0	10.0	13.0	12.1	3.1	17.1	6.3	5.0	43.6
	Corrected differential scattering cross section - $d\sigma/d\Omega$ (millibarns/steradian)									
(Total) 25-100	976 ±170	520 ±106	165 ±52	182 ±50	18.5 ±5.6	3.4 ±2.4	18.9 ±6.0	9.4 ±3.8	20.0 ±8.9	12.9 ±2.2

Elastic and inelastic scatters were not distinguishable and have not been separated. The differential scattering cross sections have been corrected for scatters hidden by the geometry and for the error in the pion count introduced by the muon contamination. The indicated uncertainties are standard deviations based upon numbers of events only. These cross sections are presented graphically in Fig. 2. It will be noted that the right-hand column includes all scatters $\geqslant 30^{\circ}$. The differential cross section in the right-hand column is, thus, the average for all angles $\geqslant 30^{\circ}$. The total counts in the 10°-15° and 15°-20° intervals should probably be reduced by two each, as a correction for π-μ decays.

Table III - Data on the Total Amount of Aluminum Traversed by the Meson Beam

Energy Interval (Mev)	Mean Energy (Mev)	Total Path of Accepted Tracks (g/cm^2 Al)	Correction for Muon Contamination (g/cm^2 Al)	Corrected Path (g/cm^2 Al)	Cross Section per Event (millibarns)
25-45	36.1	7,800	498(±33%)	7,300(±2%)	6.14
45-70	54.7	5,180	1,350(±33%)	3,830(±12%)	11.7
70-100	81.5	2,330	570(±33%)	1,760(±11%)	25.5
(Total)					
25-100	49.3	15,310	2,420(±33%)	12,890(±6%)	3.48

By "mean energy" (second column) is meant the average energy with respect to g/cm^2 of aluminum traversed. The uncertainty in total (uncorrected) path is less than one percent. The 33 percent mu contamination uncertainty is an estimated maximum. The "cross section per event" (right-hand column) was computed by assuming one event over the corrected path in each energy interval; the uncertainties are those of the corrected paths. These data, when multiplied by the appropriate numbers of events, give the respective cross sections in Tables I and II. (The total number of acceptable tracks upon which the above data are based was 3976, corresponding to 15,359 plate traversals.)

DISCUSSION

Slow Meson Nuclear Interactions.

The development of nuclear emulsions sensitive to particles of low ionization made possible the discovery of the $\pi \rightarrow \mu$ decay sequence in cosmic radiation.[4, 5] Much of the early work in the study of pion-nuclear interactions was done with these emulsions.[12] An essential difference is noted in the behavior of negative and positive pions that come to rest in the emulsions. The negative pions either produce "stars" - disintegrations of nuclei present in the emulsion - or simply disappear. The positive pions invariably decay into muons. The explanation of this difference in behavior lies in the inability of slow positive pions to penetrate the repulsive coulomb potential barrier of the nucleus. Therefore, they remain outside nuclear matter and decay into muons. The negative pion, conversely, experiences an attractive potential and is captured in a time very short compared with its decay lifetime; it just has not sufficient time in which to undergo mu-decay before being swallowed up.

Once inside the nucleus, the meson may be considered to be captured by a proton which is part of, say, a deuteron or an alpha-particle subgroup.[13, 14] The proton is transformed into a neutron ($\pi^- + p \rightarrow n$ + K.E.) that receives, as kinetic energy, half of the 140 Mev meson rest-mass energy. To conserve momentum, another particle in the subgroup, either a neutron or a proton, receives the other half of the 140 Mev - or 70 Mev. Thus, in the primary absorption event two fast nucleons, moving in opposite directions and each with about 70 Mev energy, are created. These may escape directly, leaving the residual nucleus with only a small excitation, or both primary nucleons may suffer energy degradation by collisions with other nucleons on the way out; thus causing one or two additional fast nucleons to be ejected, and/or leaving the residual nucleus in a highly excited state. This residual excitation will be dissipated by the subsequent "boiling off" of slower fragments. One of the primary fast nucleons is always a neutron (since the capture of a

negative pion is being considered) and often the other is also. In this latter event, both neutrons may escape without collisions, or may make only collisions yielding additional neutrons; and, since no ionizing particles are emitted, such an event will appear as a meson disappearance or "stop".

Fast Meson Nuclear Interaction.

The above picture (for stopped mesons) is also useful for the insight it gives into the nuclear interaction of mesons in flight. The consequences of the absorption by a nucleus of a 50 Mev "fast" meson should not be too different from those of the absorption of a "slow" meson after coming to rest. The meson rest mass will still be the major contributor to the energy released. Here there is, however, the possibility of the absorption of positive, as well as negative, pions because the repulsive coulomb potential barrier is now low relative to the pion kinetic energy; and from charge-symmetry considerations, one expects positive pion events to "mirror" negative pion events, i.e., neutrons to replace protons, and vice versa. In the case of fast mesons one, of course, expects scattering events, in addition to absorption events.

As suggested in the introduction, the artificial production of mesons into beams that could be brought outside the radiation shielding of accelerators made possible the use of cloud chambers for studying meson interactions. Electronic techniques have also been introduced by several experimenters and nuclear emulsions continue to be used. (For an excellent review article and an extensive bibliography, see Marshak.[15])

Recent work, in addition to studies on interactions with complex nuclei,[16-24] includes successful attacks using electronic techniques on meson interactions with free nucleons.[22-29] One group has even used a diffusion cloud chamber for meson-proton and meson-alpha-particle experiments.[30, 31]

Most experimenters have used pions with energies between 50 and 100 Mev. Work has been done with pions of both signs, but that with negative pions predominates. The general

features of pion interactions with a wide range of complex nuclei are shared by both positive and negative varieties. The total cross sections (in the above-mentioned energy interval) are approximately equal to the nuclear areas (geometrical cross sections); inelastic events(i.e., absorptions and inelastic scatters) occur somewhat more frequently than elastic (scattering) events; and there is a high probability for large angle, single scatters. There is at least one marked difference between the two signs, however. A large fraction of negative pion absorption events are disappearances, while few, if any, of the positive pions suffer disappearances. This difference may be understood by noting that a positive pion always produces within the nucleus at least one fast proton, while a negative pion similarly always produces at least one neutron. When the second fast nucleon is a neutron also, the negative pion may suffer a disappearance.

More recently, especially with observations on hydrogen and deuterium, it has been found that the total cross section increases rapidly with energy up to energies of 100 or more Mev. Beyond 100 Mev the cross section begins to level off.[17, 24, 25, 27, 28] At very high energies - at 920 Mev, obtained in cosmic rays - the total cross sections on carbon and lead have dropped down to about 75 percent of the nuclear area.[32]

Comparison of Results.

The results obtained in the present experiment (Figs. 1 and 2, and Tables I and II) are in general agreement with the statements made above. A direct comparison with the published data on total cross sections for aluminum can be made. Camac et al.,[20] apparently using equal numbers of positive and negative pions of about 45 Mev, obtained 480 ± 140 mb; Chedester et al.,[22] using 85 Mev negative pions, obtained 623 ± 25 mb; and Martin et al.,[23] using 109 Mev and 133 Mev negative pions, obtained 590 ± 60 mb and 580 ± 50 mb, respectively. The author's results are in agreement with these data. It will be noted that the results of Martin et al. indicate a leveling off beyond, say 100 Mev.

Camac et al.[20] have also separated star events from scattering events. Unfortunately, they did not distinguish between scatters and single-prong stars (they lumped these together) because the two kinds of events in the absence of a magnetic field had similar appearances in their cloud chamber. With this restriction they observed six stars and nine scatters $>20^{\circ}$, which is in rough agreement with the author's corrected data; i.e., 38 2-prong stars and 73 1-prong stars plus scatters $\geqslant 30^{\circ}$.

Byfield et al.[21] have made a magnet cloud chamber study of both negative and positive 62 Mev pions on carbon. They have distinguished elastic from inelastic scatters and, for positive pions, have obtained σ(star) = 153 ± 22 mb, σ(elastic scattering) = 89 ± 10 mb, and σ(inelastic scattering) = 15 ± 8 mb. If their elastic and inelastic scattering cross sections are combined, one finds the ratio of star events to scattering events to be 3:2. This is precisely the ratio the author has obtained for aluminum. A further interesting comparison can be made: Byfield et al.[21] list also the proton star prongs >40 Mev. The ratio of number of fast prongs to number of stars is 161:153 (=1.05). The like quantity for the author's experiment is 49:67 (=0.73). This difference between carbon and aluminum is not surprising; fast protons are more likely to suffer collisions and, hence, to be degraded more in energy when leaving the larger nucleus - aluminum.

In the present work, all of the 20 stops observed (i.e., disappearances - see Table I) were assumed not to be true disappearances but, rather, stars and scatters that were hidden by the geometry. This assumption seemed reasonable because all of the observed stops could be accounted for by the geometrical corrections applied to the observed stars and scatters. The validity of the assumption is further substantiated by the work of others in studies of fast positive pions in emulsions. Bernardini and Levy[17] observed no disappearances in the course of finding 41 scatters $>40^{\circ}$ and 118 stars. Similarly, Rankin and Bradner[19] discovered no disappearances while finding five scatters $>30^{\circ}$ and 11 stars.

Theoretical Models

Under "Results" it was remarked that a number of two-

prong stars were of such character that the prongs came off in approximately opposite directions. This phenomenon has been reported before,[17, 21] and it has been pointed out that this is evidence favoring a model proposed by Brueckner, Serber, and Watson.[33] These authors have suggested that a positive pion is absorbed by a neutron in the nucleus and the recoil is taken up by an adjacent nucleon. Both the neutron-turned-proton and the recoil nucleon are then ejected in opposite directions with 70 Mev kinetic energy each from their position in the nuclear structure. This is not unlike the models suggested by Perkins[13] and Tamor[14] for the absorption of stopped negative pions as referred to earlier in this discussion.

Another model which has been used to describe both scattering and absorption is that of Fernbach, Serber, and Taylor.[34, 35, 21] This is the so-called optical or transparency model. One imagines a meson plane wave impinging upon a sphere characterized by a refractive index and an absorption coefficient. The refractive index is related to the potential that the meson encounters upon entering the nucleus; the absorption coefficient is related to the absorption mean free path for mesons in nuclear matter. In such a model the meson wave experiences a phase shift and an attenuation in traversing the nucleus. The experimental dip in the differential scattering cross section found within the 60° to 90° interval (Table II and Fig. 2) could be interpreted as a diffraction minimum due to this effect. (There is possibly another dip within the 120° to 150° interval).

It will be noted that the models mentioned above use phenomenological approaches. (See also Johnson[36] for a third phenomenological model.) The necessity for such phenomenological methods is dictated by the inability of meson field theory to deal effectively with complex nuclei in a direct way. It also points to the probability that studies of the interactions of mesons with complex nuclei are more likely to yield information concerning the structure of the nucleus rather than the role of mesons in nuclear forces.

The Unusual Event.

This discussion will be concluded with a few remarks on the inelastic charge-exchange scatter ($\pi^+ + n \rightarrow p + \pi^o$) of Fig. 14. This event might also be interpreted as a radiative capture process ($\pi^+ + n \rightarrow p + \gamma$), wherein the photon is converted into an electron-positron pair in the aluminum. As Rankin and Bradner[19] have pointed out, this latter eventuality is very unlikely. The inverse photomeson production cross section is extremely small[37] and one can infer from detailed balancing arguments that radiative capture is also extremely unlikely.

The coincidence of the 1-prong star and the pair might have been accidental. This is also extremely unlikely; one can estimate the probability of an accidental coincidence from the fact that perhaps 30 high-energy pairs occurred in the 600-odd pictures scanned. If one assumes, conservatively, that the pair and the star had to intersect within the same 0.2-inch square section of aluminum plate before they would appear to be in "coincidence", then the accidental rate per star for such coincidences is 10^{-5}. This probability is reduced much more when one takes into account that all the other pairs seen in the chamber pointed back toward the CH_2 target source (Fig. 3), i.e., were produced by gamma rays originating in the cave. The pair in Fig. 14 is almost at 90^o to the target direction and could not have been created by a gamma ray from that source.

One can only conclude that the pair was the result of a neutral pion decay associated with the one-prong star. (The neutral pion mean life is less than 5×10^{-14} sec.[38] and the π^o could not have traveled more than 10^{-3} cm before decaying.) The neutral pion's normal mode of decay is into two gamma rays of 70 Mev each in the center-of-mass system. Since a radiation length in aluminum is 9.7 cm, it is readily imagined that among, say, 50 charge-exchange scatters one of the 100 photons would produce an electron-positron pair in the aluminum that could be observed in the chamber. It is, therefore, possible that a number

of the 1-prong stars observed were associated with inelastic charge-exchange scatters.

The electron pair might also have come directly from the neutral pion decay.[39] Steinberger[40] has very recently found that two percent of neutral pion decays result directly in an electron pair and a single gamma ray - in competition with the two-gamma process.

EXPERIMENTAL PROCEDURE

The experimental procedure may be divided into two parts: (1) the production and recording of events and (2) the measurement and reduction of the data.

Summary.

Briefly, π^+ mesons (positive pions) of about 50 Mev energy were produced by bombarding a polyethylene target with a 340 Mev pulsed proton beam. These pions were turned 90° magnetically and channeled through suitable collimating apertures into an array of five parallel aluminum plates inside a Wilson cloud chamber. The chamber itself was in a 5200-gauss magnetic field. Meson-induced events occurring in the chamber were recorded by a stereoscopic camera. These stereoscopic photographs were then reprojected upon a movable screen in a manner permitting the original three-dimensional configuration of events to be observed and measured. By a sampling procedure the energy spectrum and total path lengths for mesons traversing the aluminum plates were determined. Finally, after counting the events, applying certain geometrical weighting factors, and making allowances for contaminating particles in the pion beam, the desired scattering and absorption cross sections were obtained. The details of this procedure are outlined in what follows.

Production and Recording of Events.

The experimental arrangement is indicated in Fig. 3.

Production of the Meson Beam. The external deflected proton beam of the 184-inch Berkeley synchro-cyclotron traverses the concrete radiation shielding of the cyclotron through an evacuated

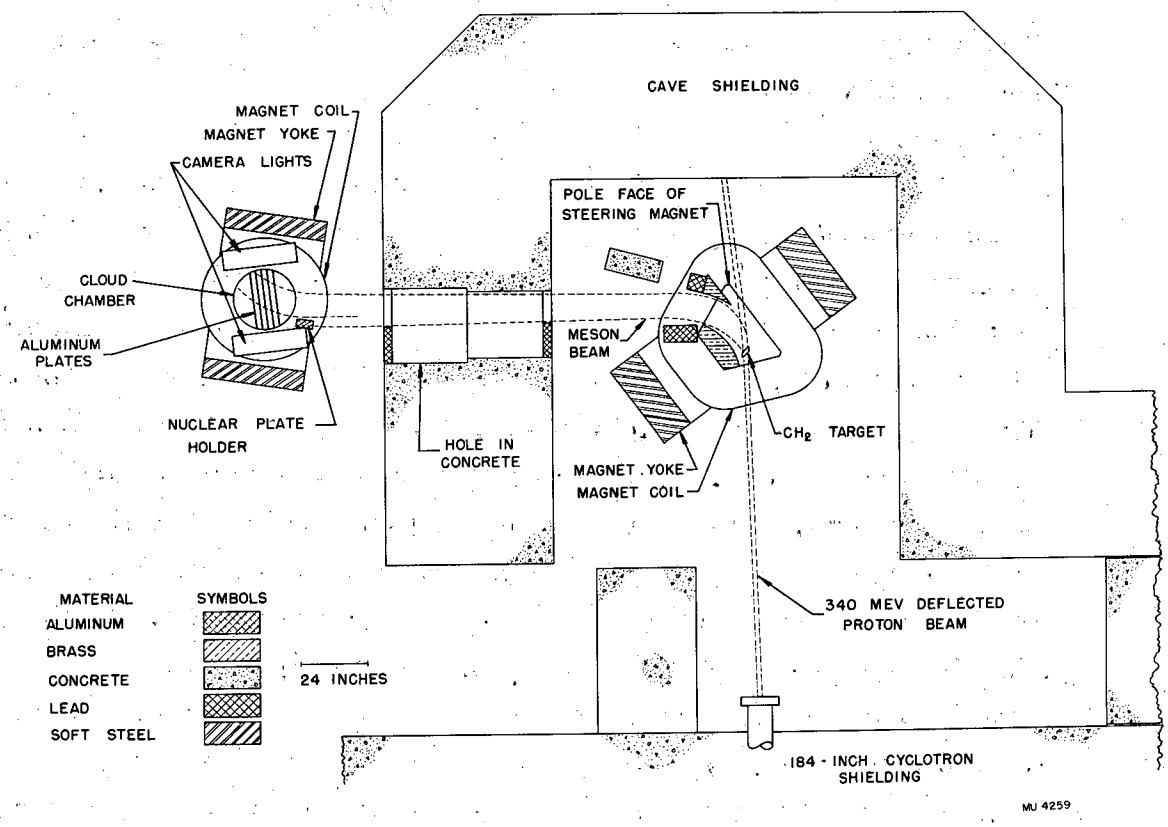

Fig. 3. - Experimental Arrangement

collimator and enters the "cave" - a small room defined by five-foot thick concrete walls - with an energy of 340 Mev[41] and circular cross section two inches in diameter. The protons were used to produce positive pions in an arrangement used by Richman, Skinner, Merritt, and Youtz.[42] The protons are caused to strike a two-inch thick polyethylene (CH_2) target. The pions of most interest are those created in the $p + p \rightarrow \pi^+ + d$ reaction which has a particularly large cross section per Mev per steradian in the forward direction.[7, 43] Pions coming off in the forward direction have a line spectrum at 69 Mev. Positive pions are also created in the reaction $p + p \rightarrow \pi^+ + n + p$, with a maximum energy of 64 Mev, and from protons on carbon in the target with energies ranging to well over 100 Mev.[44, 45, 46]

Richman, et al.,[42] also using a two-inch CH_2 target, obtained a spectrum for mesons in the forward direction peaked at 54 Mev and with a width at half-maximum of 5 Mev. The spectrum measured at the cloud chamber in the present experiment is indicated in Fig. 4; the maximum occurs at a lower energy (44 Mev) and its half width (14 Mev) is greater. The lower peak energy is partly accounted for by the 3 Mev ionization loss in the long air path (175 inches from target to cloud chamber) and the 1/8-inch plastic, cloud-chamber wall. It was, however, brought about largely by the wide acceptance angle given the meson channel at the target, as will be explained.

The energies of mesons from the p-p reaction drop off rapidly as the angle, made by the meson with respect to the incident proton beam, increases.[7, 47] It is to be expected then that the superposition of the meson energy spectra for various angles about the forward direction would produce a composite spectrum having a lower and broader energy peak, in agreement with Fig. 4. The wide acceptance angle at the target seemed necessary in order to obtain at the chamber a reasonable number of mesons (10 to 20) in each picture. In addition to its effects on the spec-

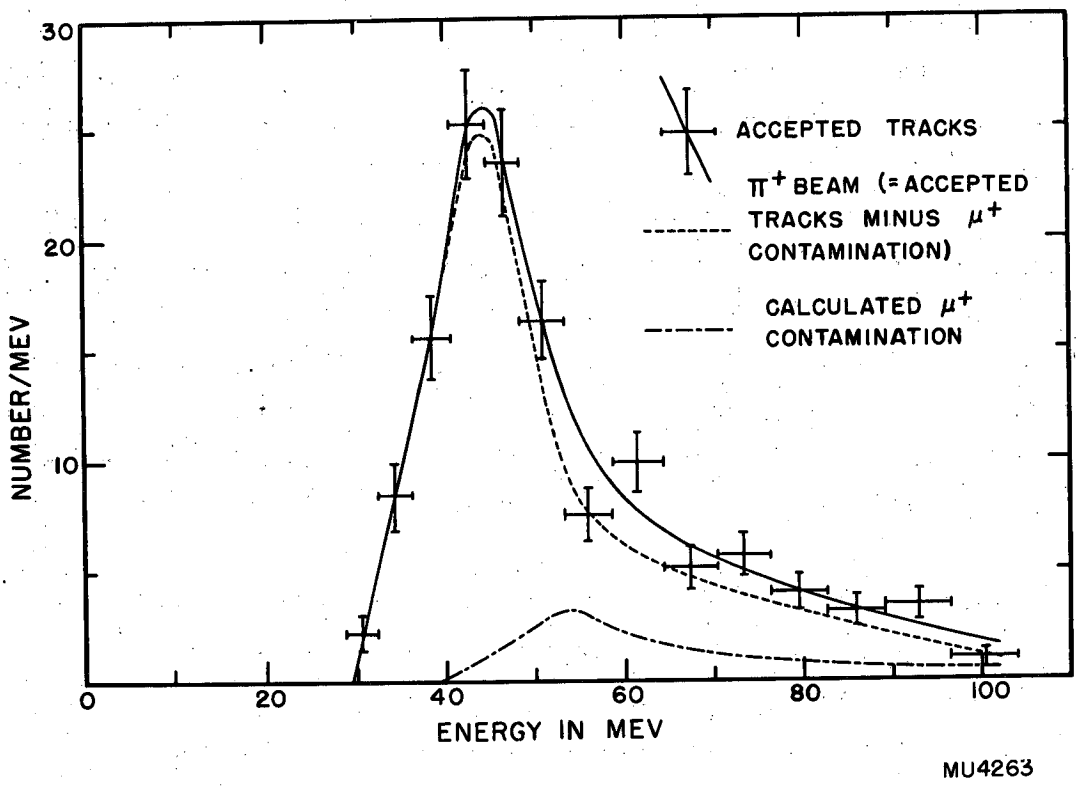

Fig. 4. - Energy Spectra for the Incoming Meson Beam

These data are based upon a sample of 628 accepted tracks measured before the first plate. Accepted tracks satisfied certain criteria regarding ionization, position, and direction intended to identify them as positive pions, but which did not exclude positrons and positive muons of acceptable Bρ. Positron contamination was negligible. The energies plotted for the μ^+ contamination are the energies of pions having the calculated muon Bρ's. Standard deviations and energy groupings are indicated for the accepted tracks.

trum, mentioned above, the wide acceptance angle allowed mesons of higher Bρ (momentum) to reach the chamber. These high energy mesons, evinced by the high energy tail in Fig. 4, were produced by protons on the carbon atoms in the target.

Beam Collimation. As indicated in Fig. 3, the CH_2 target was placed between the horizontal pole faces of a large steering magnet. The magnet air gap was 3.9 inches high and had a field of approximately 10,000 gauss, which turned the mesons through 90° and directed them out through an 8 x 24-inch tunnel in the cave wall and into the cloud chamber outside. The meson trajectories were surveyed by extending a very flexible stranded copper wire, under a measured tension, from the cloud chamber to the CH_2 target while a predetermined electric current was passed through it. The path of the wire in the magnetic field of B gauss then corresponded to that of a meson having a Bρ (=10T/I) gauss-cm; T is the wire tension in dynes and I is the wire current in amperes. The placement of the brass-lined meson channel in the magnet was determined by this survey. The channel had an aperture of 11 x 3 inches at the edge of the air gap. Lead bricks and concrete blocks were used additionally to reduce the amount of unwanted "spray" from the proton beam from reaching the chamber. Lead bricks were also used at the entrance and exit of the tunnel in the cave wall to form collimating apertures for the meson beam of 11-1/2 x 4-7/8 inches and 13 x 4 inches, respectively. (A schematic diagram of the meson beam geometry is shown in Fig. 5.)

Cloud Chamber and Aluminum Plates. The Wilson cloud chamber used (Figs. 6 to 9) was developed by Powell[48] and has been used by him an others for a number of experiments. It is 22 inches in diameter, has a sensitive region 3-1/2 inches deep, and has an expansion ratio that is pressure controlled. It fits into the six-inch gap of a magnet[48] capable of producing 22,000 gauss when pulsed and 8200 gauss in steady-state operation. A compromise 5200-gauss steady field was used in this experiment. A higher field was desirable to increase the curvature of

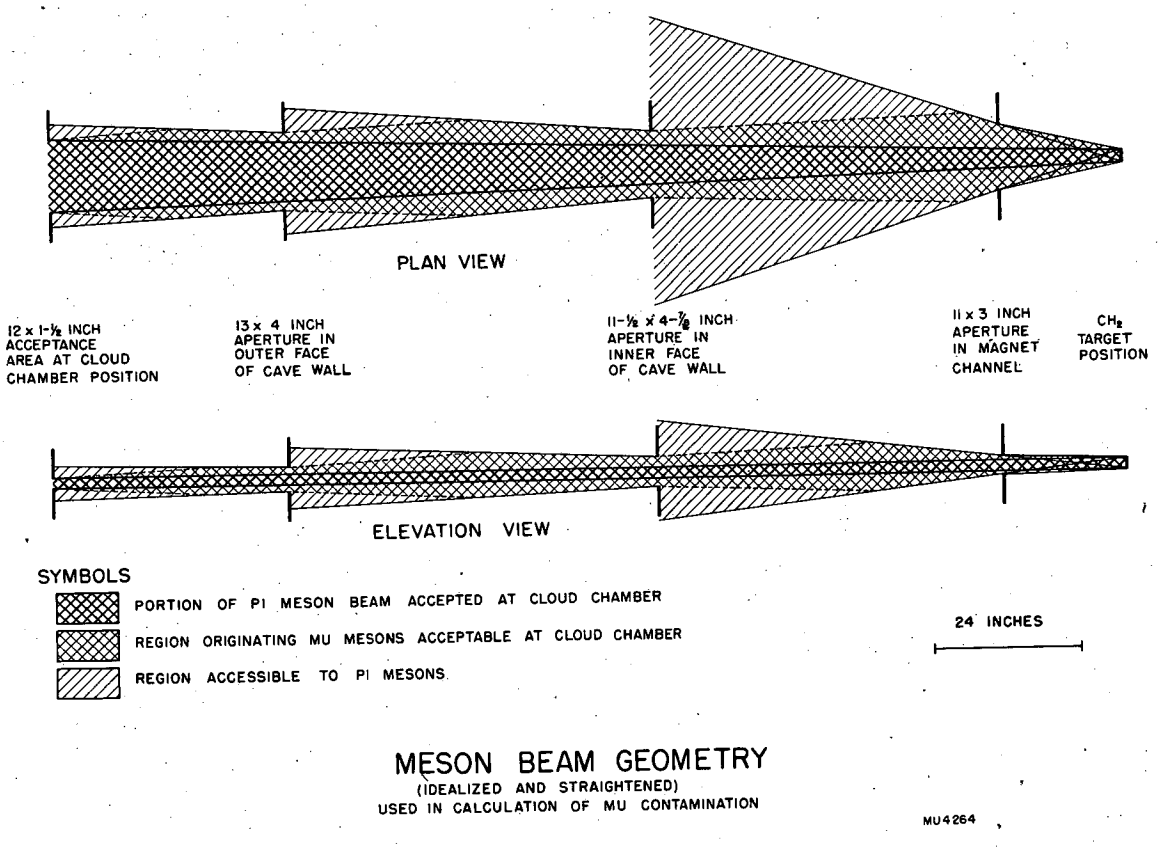

Fig. 5. - Schematic Drawing of the Meson Beam

The mesons originate in the polyethylene target at the right and travel toward the left until those which the collimation permits enter the cloud chamber. The magnetic fields have been removed in this diagram, and the actual curved paths of the particles have been replaced by equivalent straight paths.

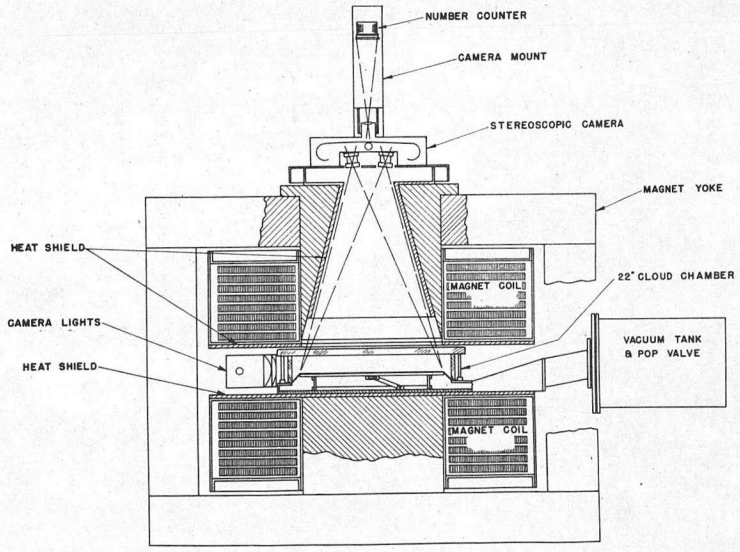

Fig. 6. - 22-inch Cloud Chamber Assembly

This schematic drawing indicates the arrangement of magnet, camera, and lights. The cloud chamber and lights shown are actually earlier versions, which have been subsequently modified slightly.

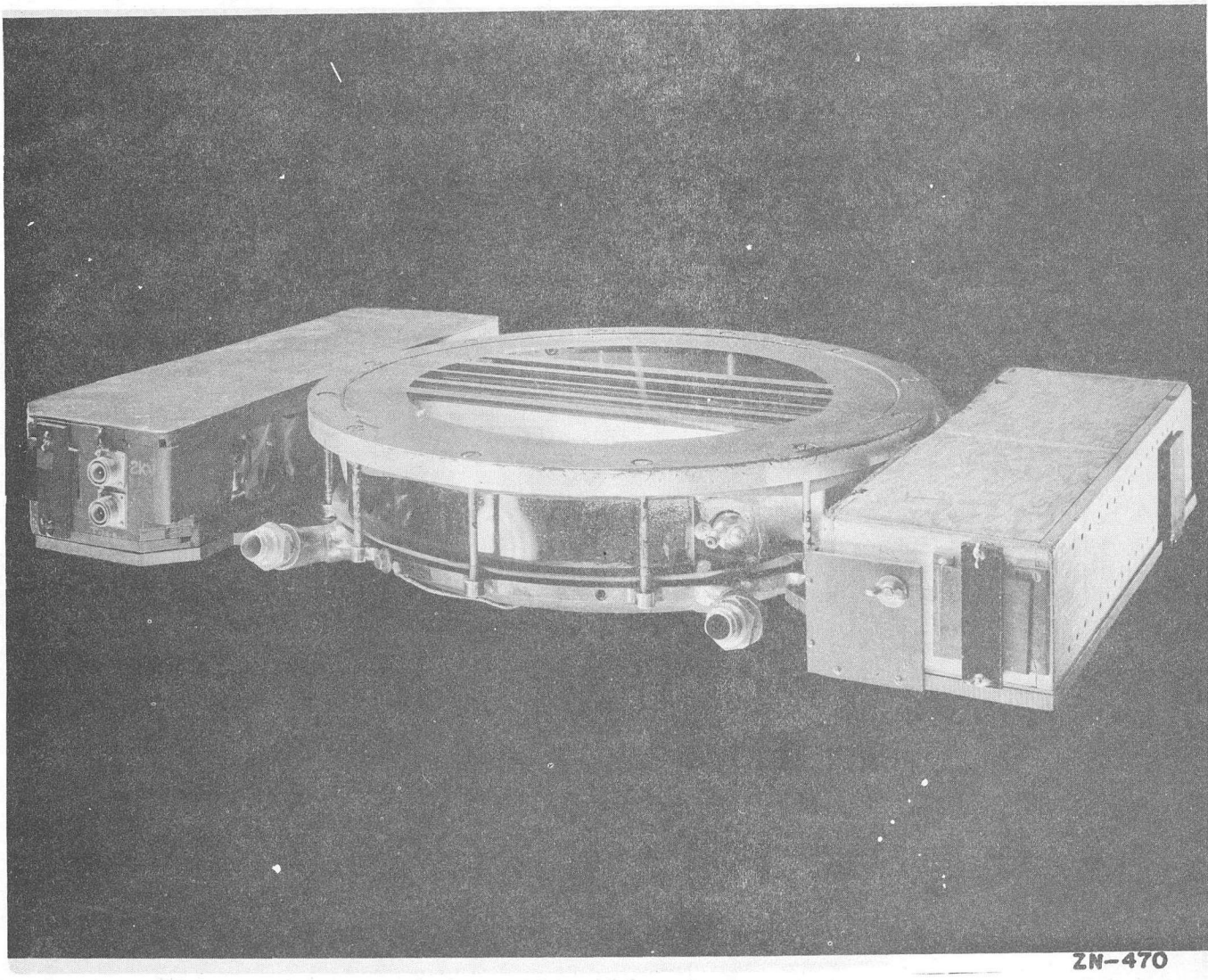

Fig. 7. - 22-inch Cloud Chamber

This view shows the light boxes at either side, and the portion of the transparent plastic cylinder through which the meson beam entered.

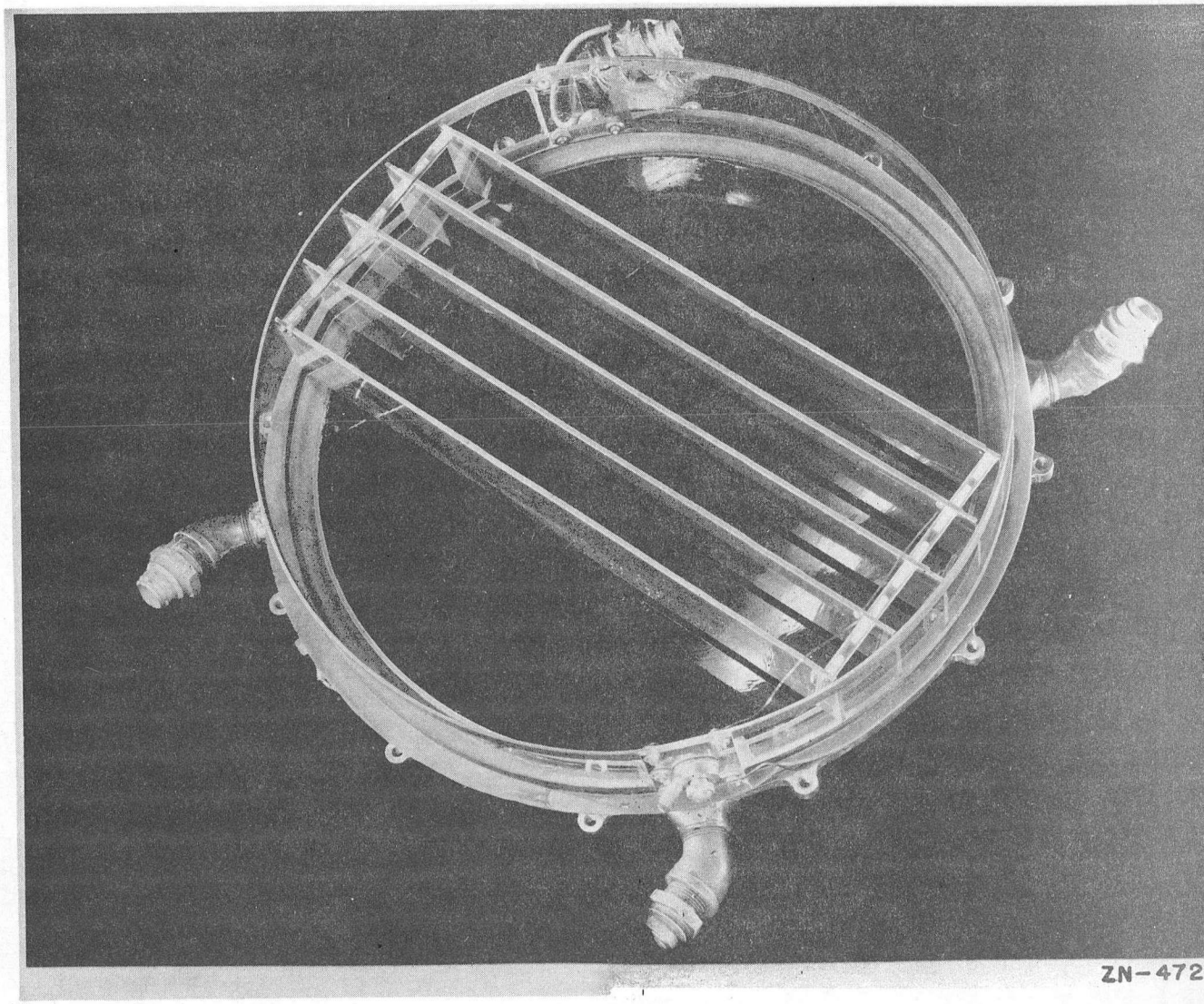

Fig. 8. - Aluminum Plate Assembly

The cloud chamber top glass has been removed to show the five 1/8-inch aluminum plates, and the 22-inch diameter transparent plastic cylinder which constituted the side wall of the chamber.

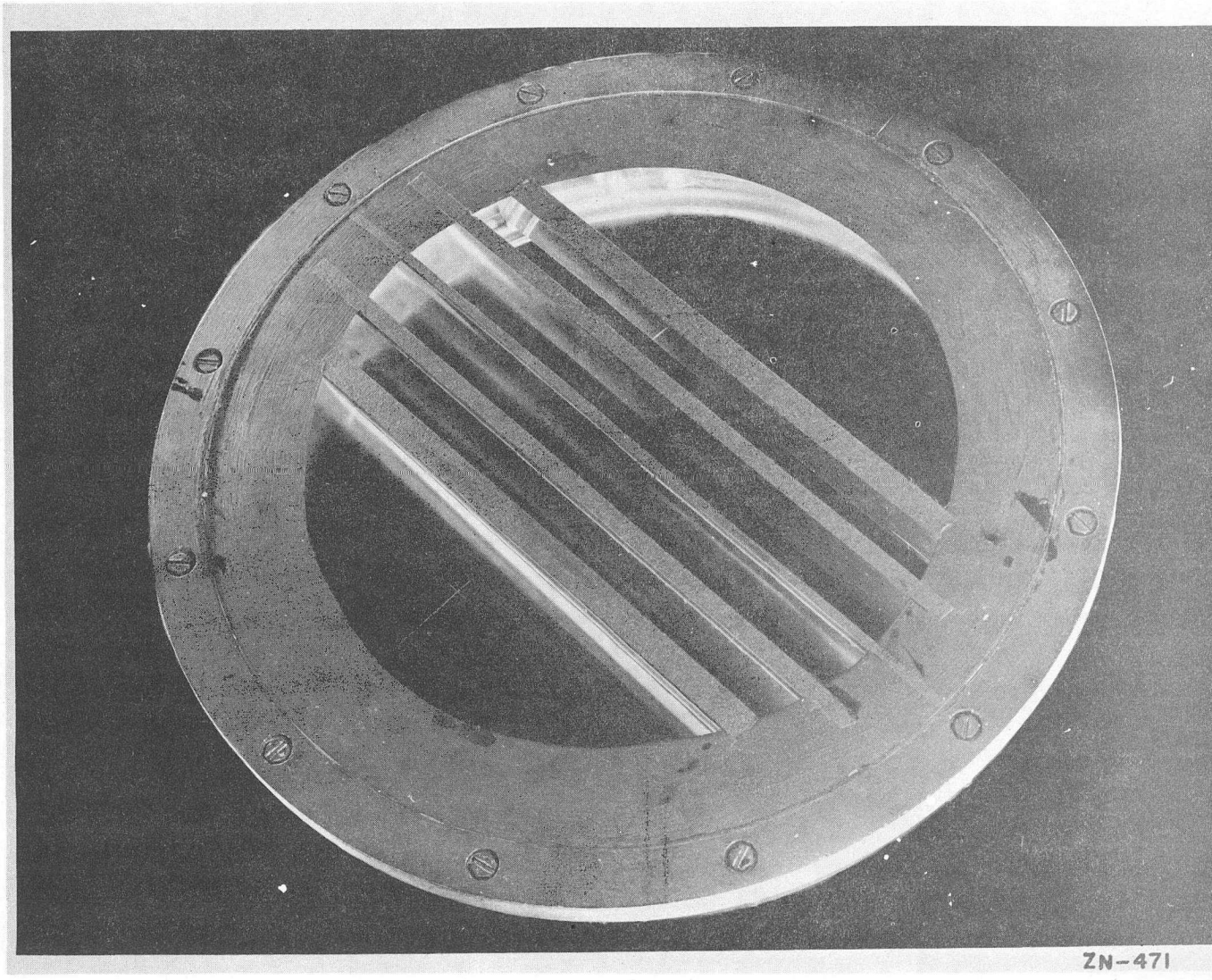

Fig. 9. - Top View of the Cloud Chamber

Shown are the strips of black masking tape placed on the upper surface of the top glass to hide the camera lenses from the light flare diffusely reflected off the sides of the aluminum plates.

the mesons and thus make possible more accurate measurements of their momentum; a lower field was needed to reduce the curvature in order that mesons might more readily enter the chamber. A lower field also has the advantage of permitting a more accurate measurement of scattering angle. The cloud chamber and light boxes (Fig. 7) are thermally isolated from the surrounding air by a half-inch thickness of felt. (1/8-inch felt was used where the meson beam entered.) It is isolated from the magnet pole faces by water-cooled heat shielding that is automatically regulated to maintain the chamber at constant temperature.

The expansion of the chamber is produced by the downward motion of a rigid circular diaphram sealed to the side walls by a ring of sheet rubber. This diaphram is coated with a 1/16-inch layer of gelatin blackened by ordinary household dress dye. Such a coating provides an excellent jet black background against which to see and photograph the tracks in the chamber because there is no diffuse reflection of light. The chamber wall is a cylinder 22 inches in diameter by 3-1/2 inches high and, in the present experiment, was formed of CR-39 transparent plastic sheet 1/8-inch thick.* This plastic sheet has excellent optical properties, is highly abrasion resistant, and is resistant to a wide variety of chemical reagents. In particular, for cloud chamber applications it resists ethyl alcohol. A major fault is the difficulty with which it is fabricated. A strip of the material 3-1/2 inches wide was closed into the desired 22-inch diameter cylinder by means of a lap joint precariously bonded with a thermosetting liquid resin.** This resin was polymerized by the addition of a catalyst and the application of moderate heat. The cylinder of CR-39 plastic sheet possesses several advantages in

---

* CR-39 plastic was developed by The Pittsburgh Plate Glass Company and is manufactured in sheet form by the Homalite Corporation of Wilmington, Dealware, and the Cast Optics Corporation of Riverside, California.

** Available under the designation "Astrolite R-350 Polyester Resin with catalyst" from the Industrial Plastics Service, Oakland, California.

comparison with the machined acrylic plastic (Lucite or Plexiglas) cylinder ordinarily used with this chamber: (1) it is thinner-walled (1/8, rather than 1/2-inch) and, therefore, the degradation in energy, of about one Mev, suffered by mesons passing through it is smaller; (2) its excellent optical surfaces permit a better illumination of the interior of the cloud chamber; and (3) its resistance to ethyl alcohol allows a mixture of ethyl alcohol and water to be used as the condensible vapor. This last advantage accrues because an alcohol-water vapor mixture necessitates a smaller expansion ratio than does water alone, or alcohol alone.[49] Argon was selected as the chamber gas because of its high specific ionization and because as a monotomic gas, it requires a still smaller expansion ratio than does a polyatomic gas. The meson tracks in this experiment were of nearly minimum ionization. Such tracks can be difficult to see, at best, and a gas of high specific ionization helps. The actual expansion ratio with argon and the ethyl-alcohol-water-vapor mixture was 9.5 percent. The expanded pressure at equilibrium temperature was 91 cm of mercury.

The five aluminum plates in which the mesons were scattered and absorbed are shown in Fig. 8. 2S, commercially pure, aluminum having a minimum purity of 99 percent was used. The plates were 1/8-inch (0.858 g/cm^2) thick, three inches high, and spaced at two-inch intervals. Their surfaces were polished to improve the illumination between the plates. An electric clearing field of 100 volts was applied between plates and between the outside plates and colloidal graphite rings painted on the inside surfaces of the plastic cylinder.

The cloud chamber was operated on a one-minute cycle that was controlled automatically. The fast timing sequence was as follows: At zero sec. the expansion was initiated, i.e., the downward motion of the diaphram was begun; at 0.042 sec. the diaphram struck bottom, i.e., stopped; at 0.046 sec. the cyclotron was pulsed and the meson beam entered the chamber; and at 0.083 sec. the lights were flashed and a photograph taken. During this fast timing sequence the clearing field was shorted out.

Camera and Lights. A conical hole in the top pole piece of the magnet permits an automatic motor-driven camera to look down into the chamber and take paired stereoscopic photographs through twin 50 mm, f/2, Leitz Summitar lenses spaced 4-1/2 inches apart. The camera is mounted 27-1/2 inches above the one-inch thick tempered plate glass top of the chamber. The photographs are taken in sequence on 100-foot rolls of 1.8 inch wide Eastman Linagraph Ortho film, which is developed to maximum contrast. The chamber is illuminated from opposite sides by "light boxes", each containing a General Electric FT422 flash tube mounted behind a row of five large spherical lenses. These lenses focus the line light source of the flash tube into a parallel beam to illuminate a region of the chamber about 2-1/2 inches deep. The 100-microsecond flash from each lamp is supplied by a 1000-microfarad condenser bank charged to 1500 volts.

Measurement and Reduction of Data.

Stereoscopic Projector. All counting and measurement of events was made from the stereoscopic photographs. These were reprojected in the stereoscopic projector diagrammed in Fig. 10. This projector has been developed for the general use of the Radiation Laboratory cloud chamber group, under Prof. Wilson M. Powell; its construction and operation have been described elsewhere.[50, 51] Briefly, the projector duplicates the optical system of the camera-cloud-chamber arrangement and permits the reconstruction, in space, of events which occurred within the chamber. This reconstruction can only be done with one track at a time and is accomplished by bringing the two track images - one from each of the two lenses - into alignment on the translucent projector screen.

The screen has three translational and two rotational degrees of freedom for this purpose. Scales are provided for reading off the height and angular positions, α and β, of the track in the chamber. The radius of curvature ρ of a track is measured by matching the track to the appropriate one of a series of template curves. These

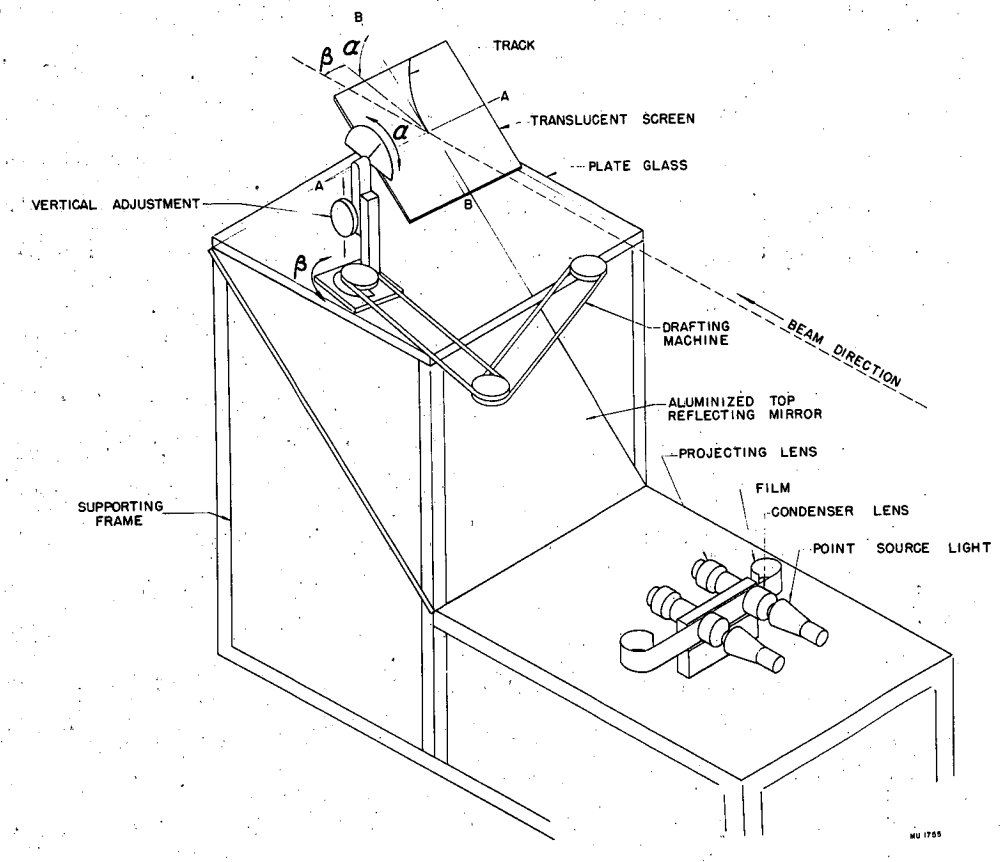

Fig. 10. - Schematic Drawing of the Stereoscopic Projector

curves are scribed in arcs of increasing radii on the surface of transparent plastic templates. The dip angle α measures the inclination of a track with respect to the vertical direction, e.g., $\alpha=90^{\circ}$ for a track lying in a horizontal plane. The beam angle β is measured in a horizontal plane, and is defined as the angle between a vertical plane normal to the aluminum plates and the projection of the track on the horizontal plane. (The normal to the aluminum plates is represented as the beam direction in Fig. 10.)

Selection of Tracks. The geometrical criteria by which meson tracks and events were accepted (or rejected) are discussed here. The section on "Meson Beam Contamination" and Appendixes I and II contain discussions of the means by which mesons were distinguished from heavier particles and the manner in which positron and mu contaminations were handled.

Acceptable tracks were required to lie within the well-illuminated region, to have sufficient track length before the first plate to permit good curvature measurements, and to satisfy certain conditions on dip angle α and beam angle β at the first plate. The region of good illumination extended over a depth of approximately 2-1/2 inches. Outside of this region tracks became more and more faint. Only those tracks and events were accepted which lay in a two-inch vertical interval beginning at one inch above the gelatin on the chamber bottom and extending to within one-half inch of the top glass. This allowed a margin of illumination for observing scatters and star fragments that were leaving the illuminated region.

Fig. 11 serves to illustrate how the first plate was divided into four intervals, I to IV, for the purpose of grouping the incoming tracks. Tracks passing to the right of I, or the left of IV, were considered too short (they were less than 7 cm long) for good curvature measurements. The vertical white lines near the right end of each plate indicate the points beyond which a track traversal was not counted; meson scatters or star fragments originating to the right of these lines were considered more likely to be obscured by the geometry than those nearer the center of the chamber, particularly,

since the view through the other camera lens shows less of the right side of the chamber than does the view shown in Fig. 11.

The acceptable values for the dip angle α were taken to be those in the range 87° to 93°, i.e., those within $\pm 3^{\circ}$ of the horizontal. All but two or three percent of the otherwise acceptable tracks lay within this range; those outside were considered more likely to be muons from the decay of pions in flight than pions themselves. This six-degree range for acceptance may appear excessive if one considers only that the cloud chamber subtended a vertical angle of less than one degree at the target; but multiple scattering in the air and chamber wall, and, particularly, the upward and downward deflections of the mesons by the small radial component of the cloud chamber magnetic field can readily account for these larger angular deviations.

The acceptable range of values for the beam angle at the first plate was determined in the following way: The tracks were separated into groups I to IV, according to their point of entry into the first plate. Tracks within each group were divided, in turn, into three radius-of-curvature subgroups. Intervals taken for ρ were 56-65 cm, 66-85 cm, and 86-125 cm. Frequency distributions for values of β were then plotted for each subgroup. These had the general appearance of a gaussian curve. In each subgroup all but about five percent of the tracks lay within $\pm 4^{\circ}$ of the average value for the subgroup. This was considered the acceptable range for pions in the particular subgroup. Mesons outside these ranges were considered to have too great a likelihood of being muons.

It should be remarked that about 10 percent of the photographs were considered to have too many tracks to be of use. That is, the tracks were so numerous that they frequently overlapped and were thus difficult, if not impossible, to follow through the aluminum plates. Such pictures were rejected without attempting to discover possible events. In this way there was no bias toward using photographs which appeared to contain events.

Sampling Procedure. The determination of an absolute cross section requires an accurate knowledge of the path length. It was considered impractical to measure the path length in aluminum.

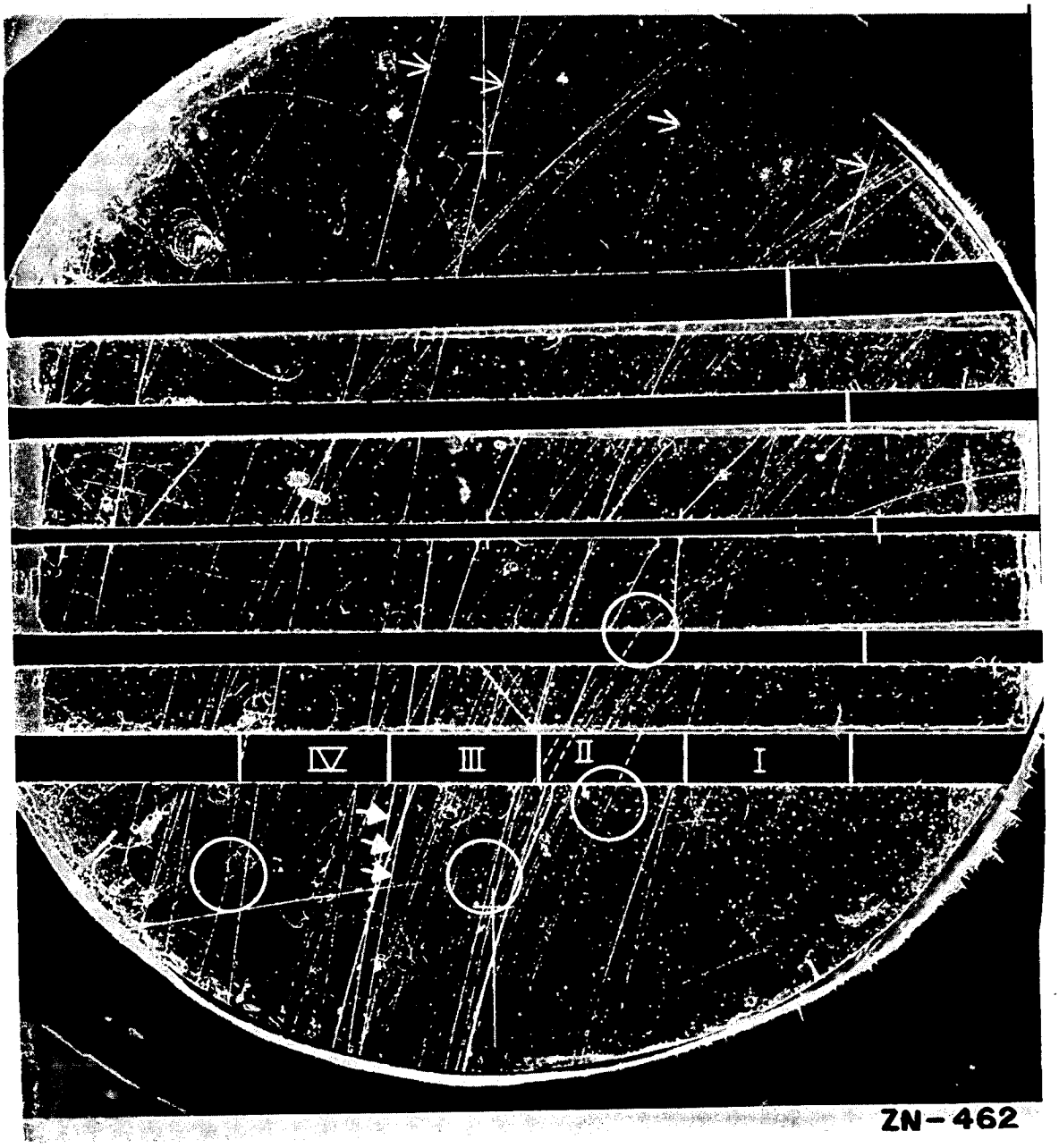

Fig. 11 - A Representative Photograph of Chamber

Aside from the exceptional number of π-μ decays (circled), this is a typical picture. The mesons enter at the bottom in thin, curving, nearly parallel paths. One π-μ decay lies under the masking tape hiding one aluminum plate, but outside the plate itself. Two others, occur in nearly vertical planes and are scarcely discernible. The four arrows $\rightarrow$ at the top indicate energetic protons (>70 Mev) that have traversed all five plates. The three arrows $\rightarrow$ at the bottom point to slower heavy particles (presumably protons) that soon stop. The thin, highly curved and spiralled tracks are electrons or (infrequently) positrons. The white bars across the plates have reference to track selection criteria. The crosses at top and bottom center are fiducial marks, spaced twelve inches apart.

for each of the nearly 4000 mesons seen in the chamber. Instead, the path length for a representative number of tracks was determined, and the data from this sample were used to predict the path length for all tracks. The various steps taken will be outlined briefly.

Approximately one-fifth of the 600-odd good photographs were selected at random and used in the sampling. These contained 850 acceptable tracks (by the criteria stated under "Selection of Tracks", above). The following data were recorded for each of 628 of these tracks: the group position (I, II, III, or IV) at which it entered the first plate; its radius of curvature ρ before the first plate; its dip angle α, beam angle β, and height H in the chamber at the point of entering the first plate; and the number T of plates it traversed before leaving the acceptable illuminated region, or otherwise leaving the region of acceptance.. For the remainder of the 850 tracks mentioned above, α was not recorded and ρ was recorded only to the extent of noting to which of the 56-65 cm, 66-85 cm, or 86-125 cm groups it belonged. A smaller random sample, of approximately 125 tracks, was used to determine the average path length per traversal through each plate as a function of group number (I, II, III, or IV) and radius ρ.

These data were then used to determine the energy distribution of the mesons before the first plate (Fig. 4) and their energy spectrum at the plate centers as a function of the number of traversals/Mev (Fig. 12). It should be noted here that, while fairly accurate ρ measurements could be made before the first plate (and after the fifth plate), it was not possible to obtain nearly the same accuracy between plates: (1) because of the shortness of the track segment available for template-matching and (2) because of the gas turbulence existing between the plates. For this reason, a meson's energy at a plate center was not determined directly from a $B\rho$ measurement, but rather by subtracting the energy lost in the aluminum from the energy it had before entering the first plate. Its energy before the first plate was determined directly from its measured $B\rho$ at that position. The energy lost in the aluminum was

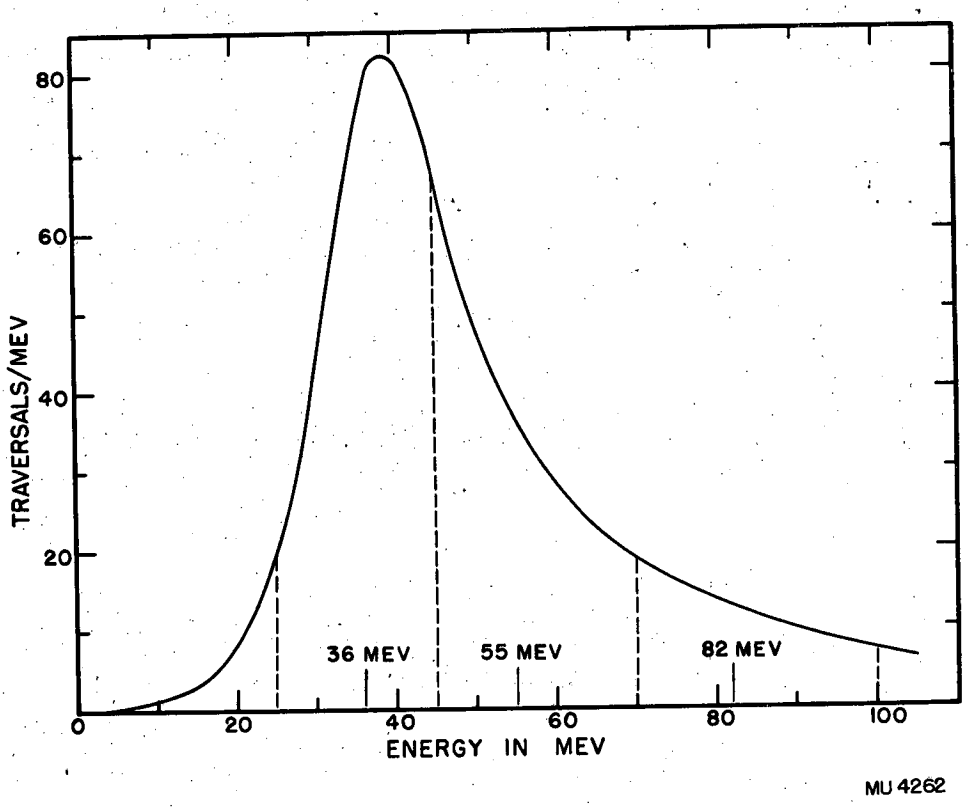

Fig. 12. - Spectrum of Meson Energies at the Centers of the Aluminum Plates as a Function of Single Plate Traversals/Mev.

These data are based upon a sample of 628 incoming tracks. No corrections for muon contamination have been made. The dashed vertical lines indicate the three energy intervals (25-45, 45-70, and 70-100 Mev) into which the data were divided for cross section determinations. The mean energy for each interval is also indicated.

obtained from the average measured path length and the range-energy relation for mesons in aluminum. The range-energy relation was obtained by converting Smith's values for protons in aluminum[52] to values for mesons (of 275 electron masses).

It will be noted in Fig. 12 that the meson energies at the plate centers have been divided into three intervals: 25-45 Mev, 45-70 Mev, and 70-100 Mev; with mean energies [= (Σ g/cm^2 of aluminum traversed x energy in Mev)/(Σ g/cm^2 of aluminum traversed)] of 36, 55, and 82 Mev, respectively. Cross section determinations were based upon the predicted total g/cm^2 of aluminum traversed in each of these energy intervals, determined by a direct summation of the sampled path lengths within each energy interval and not by integration under the curve of Fig. 12.

Rapid Count. The great majority of tracks were enumerated by a "rapid count" procedure. That is, the stereo-photographs were viewed in the projector as in the sampling procedure above, but a detailed measurement of each track was not made. It usually was possible by a visual inspection alone to determine whether or not a track met the criteria for acceptance. In doubtful cases - amounting to approximately ten percent of the total number - detailed measurements were made. The rapid count covered all pictures used, including those gone over in the detailed count under the sampling procedure outlined above. A comparison of the number of tracks enumerated in the detailed count (850) with those in the rapid count (851) covering the same random sample of photographs established the validity of the procedure.

3976 tracks (making 15, 359 traversals) were enumerated in the rapid count. The factor 6.33 (= 3976/628) was used to convert path lengths determined in the detailed count to path lengths of all tracks in the rapid count.

Counting of Events. Events (scatters $\geqslant 10^{\circ}$, stops, and stars; (see Figs. 14 to 20 for illustrative examples) were looked for by carefully following in the stereo-projector each of the 3976 tracks, along its course through the aluminum, until it either; (1) success-

fully traversed the five plates, (2) finally travelled out of the acceptable region in the chamber, or (3) initiated an event in one of the plates. (Rarely, a pion would decay into a muon between plates. Plate traversals by such muons were not, of course, considered.) Every pion initiating an event (3) was measured in detail, in the way discussed under "Sampling Procedure." In addition, the position and characteristics of the event itself were determined, especially, the angular relationship of the incoming and outgoing tracks. The coincidence of incoming and scattered meson, or incoming meson and outgoing disintegration fragments, within an aluminum plate was carefully verified. This could be done to within ±0.1 inch vertically and ±0.05 inch, or better horizontally. Stops were examined carefully to be certain that no nearby tracks might have originated from the place of disappearance.

An important point, although it was possible to distinguish a scattered meson from a one-prong disintegration by the difference in ionization, it was not usually possible to establish the scattered meson's, or disintegration (star) fragment's, energy with any precision. Again, this was because of the short path length and the gas turbulence between plates. In a few exceptional cases where the scattered meson or star fragment entered the region before the first plate or after the fifth plate (e.g., see Figs. 15 and 16) good curvature measurements could be made. There were not enough of these to be statistically significant. In most cases, order-of-magnitude estimates of energy could be made, particularly in the case of star fragments, by observing the ionization of the track and/or the change in ionization after passing through an aluminum plate. One had to be careful here because of the many variables, such as illumination which relate apparent track density to actual specific ionization loss.[49, 51]

As a check on the reliability with which tracks and events were counted, about five percent of the photographs were examined independently by two different persons. There was essentially good agreement between the independent counts.

MESON BEAM CONTAMINATION

Not all the particles entering the cloud chamber were pi mesons. It was necessary, of course, either to be able to recognize the contaminating particles or to have available information from which their numbers could be determined in order to evaluate the cross sections correctly. Among the possible ionizing contaminants were protons (and heavier particles), mu mesons, and positrons. Except for a small background of extraneous tracks produced in the chamber by them, the non-ionizing neutrons and gamma rays presented no difficulty. The few negative particles observed, presumably electrons, presented no problem either, since they were readily detected by their negative curvatures.

Protons.

Protons constituted approximately one-fourth of the particles in the beam and were differentiated from mesons by their much higher specific ionization and/or greater radius of curvature. Most had a radius greater than 200 cm, whereas the acceptable (meson) radii ranged from 58 cm through 125 cm. On the other hand, protons (in the 58 to 125 cm range), when compared with pions of the same curvature, have more than ten times the specific ionization of the latter. In either case, they could be recognized as protons (or heavier particles) and not accepted in the meson count. The data for the calculation of energy, $B\rho$, specific ionization, and range were taken from Smith,[52] as previously noted, and from Aron, Hoffman, and Williams.[53] A general discussion of the ways in which the above four, and other, quantities may be used to identify particles in cloud chambers is available elsewhere.[49, 51]

While protons are readily distinguished from pions of the same $B\rho$, muons and positrons are not. For the $B\rho$ range of values of interest in this experiment, pions have a specific ionization not more than 150 percent that of muons of the same radius and not more than two times that for positrons (or electrons) of the same radius. For this reason it was not possible to distinguish the latter two particles from pions. The extent of the muon and positron contami-

nation was determined indirectly.

Mu Meson Contamination.

The muons in the meson beam originated from the decay of pions in flight. In principle, it is possible to determine the muons expected to enter the chamber if, among other things, one knows the experimental geometry and the pion beam intensity, energy spectrum, and decay constant. In practice, it was necessary to use a number of simplifying mathematical approximations and to make certain assumptions concerning the pion beam intensity and energy spectrum. These are outlined in Appendix I. The mean life of the positive pi meson was taken to be 2.55×10^{-8} sec.[54-57] The "equivalent energy" distribution obtained for the muons contaminating the beam is indicated in Fig. 4. (By "equivalent energy" is meant that energy which a pion would have if it had the same $B\rho$ as that of the muon being considered.) The number of muons was computed to be 13 percent of the total number of pions in the meson beam. Because of large uncertainties that entered into the computations this figure may be in error by ±33 percent.

In addition to calculating the muon content of the beam, a direct measure of the contamination was attempted in two ways: (1) by ascertaining the ratio of muons to pions stopped in nuclear emulsions placed in the beam and (2) by counting the π-μ decays occurring before the first plate in the chamber; inferring from these data the total number of pions which must have entered, and comparing the inferred number with the number obtained by actual count. The statistics obtained with these methods were too poor to do more than indicate no lack of agreement with the calculated contamination. These two methods are briefly discussed in Appendix I, also.

Positron Contamination.

It has been possible to place an upper limit on the positron contamination. This limit was obtained by imagining all the particles in the beam that were accepted as mesons to have been positrons instead, and computing, from data available in Heitler,[58] the number of times these positrons would be expected to radiate more

than three-fourths of their energy in traversing an aluminum plate.

Any positron undergoing such a radiative loss would have emerged from the plate with its radius of curvature reduced in direct proportion to its loss of energy, but with no significant change in its specific ionization; no such events were observed. Such an event would have been readily recognized for what it was and could not have been confused with the inelastic scattering of a pion, even though these two basically different types of events do have some similarities in appearance. A pion suffering such a large change in radius would also undergo a large and discernible change in specific ionization.

The calculations pertaining to the positron contamination are presented in Appendix II.

GEOMETRICAL CORRECTIONS

One observes three types of meson-induced events in the aluminum plates: (1) scatters, (2) disintegrations, or "stars", and (3) stops. Type 3 presumably might represent: either (a) a real stop involving charge-exchange scattering, the emission of a neutral pion and no charged particles; (b) a real stop involving meson capture and the subsequent emission of only neutrons and slow charged particles of insufficient energy to escape the aluminum; or (c) a pseudo stop, corresponding to types 1 or 2, above, in which the outgoing charged particles are hidden by the geometry. It is possible, in principle at least, to take the observed events of types 1 and 2 and calculate, from geometrical considerations, the most probable additional number of events which would have appeared as pseudo stops. Where one is dealing with pions of positive charge few, if any, real stops corresponding to case (b) are expected. One imagines the incoming positive pion to be absorbed by a neutron within the nucleus and to give rise to at least one fast proton, which should give rise to a star of at least one prong. (Refer to comments under "Discussion - Comparison of Results".) Then the difference between the observed stops (3) and the number of pseudo stops (c) predicted by geometrically-based calculations should approximate

the number corresponding to case (a), charge-exchange scattering. Even in case (a), of course, a neutron is converted into a proton which, if given sufficient energy, will escape and give rise to a 1-prong star.

By idealizing the geometry somewhat and constructing a simple "analog computer" (Fig. 13), the evaluation of the geometrical corrections was made with a minimum of effort. The procedure used is summarized in Appendix III.

ERRORS

The probable errors in the energy determinations are estimated to have been less than five percent. Errors in cross section determinations were, in most cases, much less than the statistical uncertainties. For convenience of discussion, errors have been divided into those affecting energy determinations and those affecting cross section determinations.

This has not been a "precision" experiment; the statistics have not required precision measurements. When less than 200 events of all kinds are subdivided into half a dozen groups according to energy and character of event, as they have been here, the statistical uncertainties (of the order of 20 percent) loom large compared with all but the largest of other errors.

In Energy Determinations.

Events were grouped into three large intervals: 25-45 Mev, 45-70 Mev, and 70-100 Mev, according to the energy of the initiating pion (see Fig. 12). There is almost a 2:1 energy range in the first group, and approximately 3:2 in the second and third groups. It can thus be appreciated that only the larger errors in energy determinations are of significance.

The important quantities bearing upon the accuracy of the energy determinations are: mass of the meson, radius of curvature, magnetic flux density, rate of energy loss in aluminum, and path length in aluminum. (Compare the discussion under "Experimental Procedure - Sampling.") The present uncertainty in the positive pion mass is about one percent.[59, 60] The mass has been taken to be 275 electron masses for purposes of calculation in this experi-

ment. The true radius of curvature ρ of a track may be obscured by multiple coulomb scattering in the gas, turbulence in the gas, and errors in fitting template curves to the tracks. The probable error owing to multiple scattering has been calculated according to Bethe[61] and is about two percent for 50 Mev pions over a 10-cm path in argon at a pressure of 91-cm of mercury, the conditions obtained in the experiment.

The effect of gas turbulence was obtained by measuring the curvature of tracks photographed with the magnetic field turned off. In the absence of turbulence (and multiple scattering) these tracks should have been straight. The minimum radii obtained were of the order of 1200 cm, indicating a maximum error from this source of five to ten percent for mesons in the range of energies measured (ρ = 60 to 125 cm). Most of these "no field" tracks, however, had radii $\gtrsim$ 2500 cm, indicating that the errors were generally much smaller. The curvatures were equally divided among those of positive and those of negative sign.

The radii of the template curves, used in matching track curvatures, increased by approximately five percent increments between successive curves. Often it was possible to decide with good conscience that only one curve was a best fit or, at worst, that the choice lay between one of two adjacent template curves. The uncertainties here were, thus, of the order of three to five percent. In infrequent cases - near the edge of the chamber where track lengths before the first plate were 7 cm long instead of the usual 10 cm, and, particularly, for the large radii of 100-125 cm - it was not possible to decide among less than five or six successive curves; these lead to uncertainties of as much as 15 percent.

The magnetic flux density B was known to about one percent. There was, however, a ten percent variation in B over the region in which curvatures were measured. Because greater accuracy did not seem warranted, and for convenience in tabulating the data, this field variation was divided into two five-percent intervals; all

tracks were assigned to one or the other interval. Thus the maximum uncertainty in the magnetic field intensity was three percent.

One can readily believe that the error in $B\rho$, compounded, as it is, of the several errors discussed above, may be large in particular instances. On the other hand, these errors have equal probability of being additive or subtractive and, when averaged over a large number of measurements, tend to cancel one another. It would seem reasonable to estimate that the probable error in energy determination owing to average errors in $B\rho$ was less than five percent.

$B\rho$ determinations were only made on tracks before they entered the first plate. The separation was too small and the turbulence too great between plates to permit satisfactory determinations there. In order to fix the energy of a meson beyond the first plate, i.e., at the centers of succeeding plates, it was necessary to calculate the loss of energy by ionization in the aluminum and to subtract this loss from the meson's energy before it entered the first plate. Errors introduced by ionization-loss calculations were quite small percentage-wise because: (1) the average path lengths and the rate of energy loss were known within one or two percent, and (2) the total ionization loss in passing through even five plates was usually a small fraction of the total meson energy. This ionization loss amounted to 10 percent for 100 Mev pions and 36 percent for the lowest energy (41 Mev) pion that was accepted after traversing five plates. (No pions were accepted whose energy had dropped to less than 25 Mev.) Thus the ionization-loss calculations introduced an average error in the energy at the center of a plate which was perhaps one percent under the worst circumstances, and usually much less. It is concluded that the overall probable error in the energy determinations was less than five percent.

Uncertainties in the Cross Sections.

The calculation of the cross sections depended partly upon knowledge of the amount of aluminum traversed. Because the path length, including the contribution from contaminating particles, was determined to within one percent and the density of the aluminum to within 0.1 percent; the important cross section uncertainties depend-

ed entirely upon the statistics (see Table I), upon the reliability with which the events were counted and identified, and upon the effect of the muon contamination. (The plates had a minimum purity of 99 percent aluminum. It is presumed that the interaction effects on a per-nucleon basis are not too markedly different for the impurity atoms than for the aluminum atoms and that, therefore, there should be no need for making corrections because of the impurities.)

Each photograph was scanned very carefully for events and it is not believed that more than one or two events, at the most, were overlooked among the 111 stars and scatters $\geqslant 30^{\circ}$. Those events most likely to have been overlooked were small scatters $<20^{\circ}$ (these were not used in the calculation of absolute cross sections) and stops that were obscured by overlying tracks. Large angle scatters and stars usually stood out very clearly. There was some uncertainty, in one or two instances, concerning whether what appeared to be a one-prong star was actually a forward scatter and vice versa. These were cases where the outgoing particle was short and disappeared into the poorly illuminated region of the chamber in such a way that estimates of ionization and curvature were difficult to make.

The muon contamination may introduce errors (1) by increasing the measured total path length in aluminum and (2) by creating spurious events. The path length was corrected for muon contamination, as indicated in Table III. The 33 percent uncertainty in the contamination is an estimated maximum and leads to uncertainties in the path length (as large as 12 percent for the 45-70 Mev interval) that approach the lowest value for the statistical uncertainties (±16 percent for σ_{total} in the 45-70 Mev interval, compare Table I.) In most cases, however, the statistical uncertainties are considerably greater than those brought about by the mu contamination.

It has been shown by other experimenters that the interaction between muons and nucleons is very weak,[62, 63] certainly much less than a millibarn. It has been assumed, therefore, that no disintegrations nor large-angle scatters were muon-induced.

There was no possibility of a π-μ decay in an aluminum plate contributing to the observed scattering count for angles $\geq 30^{\circ}$; the maximum π-μ angle is 26° for a 25 Mev pion, and only 18° for a 50 Mev pion. One may estimate from the angular distribution of the 31 π-μ decays observed before the first plate and the average length of tracks before the first plate relative to the average path length through the plates that two π-μ's contributed to the count of scatters between 10° and 15°, two contributed to those between 15° and 20°, and none contributed to those $>20^{\circ}$. (These numbers, however, have not been subtracted from counts shown in Table II.)

One should also discuss errors entering into measurements of angles. The calculated scatter angles were based upon measurements of dip angle α and beam angle β for incoming and outgoing tracks. (See "Experimental Procedure - Stereoscopic Projector" for definitions of these angles.) β could, in most cases, be measured to within one degree. In optimum cases α could also be measured to within one degree. For steeply slanting tracks, however, the uncertainty was sometimes greater, possibly 3°, or even 5°. Larger errors were introduced in the true scatter angle by the multiple coulomb scattering of the pions in the aluminum plates. The r.m.s. value of this error for 40 Mev pions traversing one plate is about 4° and for 70 Mev pions it is about 2°.[64] These errors in angle are not important, however, in view of the 30° intervals into which scattering events were grouped.

Summing up this discussion of errors, it is believed that the statistical uncertainties quite outweight other sources of error in the cross section determinations.

ACKNOWLEDGMENTS

The author wishes to acknowledge his indebtedness to Professor Wilson M. Powell for suggesting the experiment; for making available the extensive facilities of the University of California Radiation Laboratory cloud chamber group; and particularly for his counsel, continuing interest, and active participation during the entire program.

One cannot, of course, begin to name the numerous persons whose contributions in one way or another made possible the success of this essentially complex experiment. The author's efforts, though necessary, have been but one link in a chain of many links. Thanks are due the author's colleagues in the cloud chamber group; Messrs. John B. Elliot, Franklin C. Ford, Milton M. Hill, Peter H. Moulthrop, and Dr. Peter E. Tannenwald furnished valuable technical assistance; Mrs. Dorothy J. Gardner developed the stereoscopic negatives; Mrs. Gardner and Mr. Elliot assisted with measurements of some of the data; Mr. Donald B. Johnson performed some of the computations concerning the π-μ decay energetics; and Mrs. Marguerite H. Lemmon prepared prints of the meson-induced events used as illustrations. Mr. Albert J. Oliver developed the nuclear emulsions.

This work was performed under the auspices of the United States Atomic Energy Commission.

APPENDIX I

EVALUATION OF MU MESON CONTAMINATION

By Direct Calculation.

The beam geometry is displayed in Fig. 5 and was used in calculating the distribution of the mu meson contamination. To simplify the computations, the magnetic fields at the CH_2 target and at the cloud chamber (see Fig. 1) have been assumed removed and the meson paths have been approximated by equivalent rectilinear paths. The geometry is otherwise that actually used during the experiment. The pi meson beam originated at the CH_2 target and has been assumed to have had a uniform angular distribution over the region of interest in this calculation. Its energy distribution at the target was assumed to have been such as to give it the energy distribution at the cloud chamber that was measured experimentally (see Fig. 4).

As can be seen in Fig. 5, the solid angle $\omega_\pi(x)$ for pions that may decay into muons is much greater than the solid angle ω_c for pions that may enter the cloud chamber. On the other hand, only a portion of the muons originating in the pi meson beam actually enter the chamber. And some of these were rejected during the counting of tracks because their dip angles α deviated by more than $\pm 3^\circ$ from the horizontal and/or their beam angles β deviated by more than $\pm 4^\circ$ from the experimentally measured mean value. The procedure used in evaluating the amount of the contamination is outlined below. An explanation of the symbols used is appended to this Appendix.

The pion intensity per Mev at any point is

$$I_\pi(x, T_\pi) = I_\pi(0, T_\pi) \exp\left[-\lambda(T_\pi)\, x\right]$$

The relative number of pions per Mev decaying in the interval between x and $x \pm dx$ and yielding muons that might be accepted at the chamber is

$$I_\pi(x, T_\pi)\, \omega_\pi(x)\, \lambda(T_\pi)\, dx$$

The number of muons (per pion Mev) actually accepted at the chamber is

$$N_\mu(T_\pi, T_\pi') = \int_0^{x_c} I_\pi(x, T_\pi)\, \omega_\pi(x)\lambda(T_\pi)P_\mu(T_\pi, T_\pi')\omega_\mu(x)dx$$

These are muons of equivalent energy T_π' originating from pions of energy T_π. The number of pions (per Mev) of energy T_π' accepted at the chamber is

$$N_\pi(x_c, T_\pi') = \omega_c I_\pi(0, T_\pi') \exp\left[-\lambda(T_\pi')x_c\right]$$

The fractional muon contamination among pions of energy T_π' is then simply

$$C(T_\pi') = N_\mu(T_\pi, T_\pi')/N_\pi(x_c, T_\pi')$$

The integrand in the expression for $N_\mu(T_\pi, T_\pi')$ is discontinuous in x. Over certain ranges of x it was found impossible to integrate explicitly. An approximation was therefore used which replaced $\omega_\pi(x)$ by the geometric mean of its extreme values within each interval between discontinuities; the same approximation was used for $\omega_\mu(x)$. The errors introduced were of the order of one percent. These errors are small compared with those owing to uncertainties and approximations in the geometry.

With Nuclear Emulsions.

Ilford C.2 nuclear plates were buried in an aluminum block, at an angle of 15° to the horizontal, directly in the path of the meson beam and just before the cloud chamber (Fig. 3). Mesons traversed the block horizontally; those that stopped in the emulsion were those that happened to enter the block at the proper level to travel through the correct amount of aluminum necessary to remove all their energy by the time they had reached the emulsion. These stopped mesons were searched for with the aid of an oil immersion microscope. This is a well-established technique; stopped mesons have a very characteristic appearance that readily distinguishes them from protons and heavier particles, and the distance the mesons have traveled in the aluminum block furnishes a good measure of their initial energy.

Positive muons are distinguished from positive pions by the fact that the latter decay into a 4 Mev muon which proceeds characteristically from the end of the stopped pion, while the muons simply stop with no visible decay product. (Electrons are no problem be-

cause the Ilford C.2 emulsion is insensitive to them.)

In order to be certain that a muon entered the aluminum block from the meson beam and did not originate locally from the π-μ decay of a stopped pion it was required (1) that it be travelling in a generally forward direction and (2) that it traverse at least 650 microns of emulsions before stopping. (The range in emulsion of muons originating from stopped pions is 600 microns.) The same restrictions, (1) and (2) above, were placed upon pions accepted in order not to discriminate against muons. Two muons and 16 pions meeting the above criteria were found after more than two weeks of scanning. (A great many more mesons of both kinds were found whose ranges in the emulsions were less than 600 microns.) Because of the scarcity of data it was not deemed profitable to spend more time in scanning. This ratio of one-in-eight is in agreement with the 13 percent figure obtained for the contamination by direct calculation - though the statistics, of course, are exceedingly poor.

By π-μ Decays Before the First Plate.

The number of π-μ decays (from acceptable pions) observed in the chamber before the first plate in the chamber was compared with the number expected from the number and spectrum of tracks accepted as mesons. π-μ decays after the first plate were not considered, both because of the difficulty of finding them and because of the uncertainty in the path length over which they could be observed.

The average path length before the first plate along which a decay might be observed was determined, by measurement, to be 9 cm. 31 π-μ events were observed. A calculation based upon a mean life for the positive pion of 2.55×10^{-8} sec. indicated that one should have seen 47 π-μ decays if all the 3976 accepted tracks had been pions. Some would not have been observed, however, because of a decay angle so small as to escape detection. A plot of the angular distribution of the 31 observed decays indicated that angles $< 4^{\circ}$ were not observed and, further, that when the decay angle was largely in the vertical plane angles $< 6^{\circ}$ were not observed either. Corrections for these figures reduced the expected count from 47

to 39. This is 26 percent greater than the 31 actually observed. Because of the errors inherent in the above computations and because of the poor statistics, one cannot consider this percentage to be in disagreement with the 13 percent figure obtained by the more elaborate direct calculations.

Nomenclature.

c	velocity of light
$C(T_\pi')$	fractional mu meson contamination, expressed as the ratio of muons of equivalent energy T_π' accepted at the chamber relative to pions of energy T_π' accepted at the chamber.
$I_\pi(x, T_\pi)$	relative intensity per Mev per steradian of pions at position x and of energy T_π.
$N_\mu(T_\pi, T_\pi')$	number per (pion) Mev of muons of equivalent energy T_π' that are accepted at the chamber and that decayed from pions of energy T_π.
$N_\pi(x_c, T_\pi')$	number per Mev of pions of energy T_π' accepted at the chamber
T_π'	equivalent muon energy, i.e., the energy of a pion whose momentum (or $B\rho$) is the same as that of the muon being considered.
x	distance along pion path measured from the CH_2 target. (x=0) is the CH_2 target position ($x = x_c$) is the cloud chamber position.
β	(=v/c), ratio of pion velocity relative to velocity of light.
γ	$(1 - \beta^2)^{-1/2}$
$\lambda(T_\pi)$	$(= [\tau \beta \gamma c]^{-1})$, reciprocal mean decay path length for pion of energy T_π.
τ	pion mean life.
ω_c	solid angle as seen from the CH_2 target, for acceptance of pions at the chamber.
$\omega_\mu(x)$	solid angle into which muons originated at position x for pions that may decay into muons acceptable at the chamber.
$P_\mu(T_\pi, T_\pi')$	probability per steradian for a muon, of equivalent energy T_π' of moving in the forward direction after originating from a pion of energy T_π.

APPENDIX II

EVALUATION OF POSITRON CONTAMINATION

A typical energy with which pi mesons traversed the aluminum plates is 50 Mev (see Fig. 12). A positron of the same Bρ (momentum) as a 50 Mev pion has an energy E of approximately 125 Mev.

One wishes to determine the probability that such a 125 Mev positron will radiate more than, say, three-fourths of its kinetic energy while traversing these same aluminum plates. If one considers a large group of positrons (of energy E Mev) passing a cumulative distance L cm through an absorber having N atoms per cm^3, one may write $W = ELN\theta_{rad}$, where W is the cumulative energy (in Mev) lost by radiation by the group, and θ_{rad} is the cross section (in cm^2/atom) for loss of all the positron's energy by radiation. One further wishes to obtain the proportion of this cumulative radiation loss W which goes into producing quanta having energies lying between 3/4 E and E.

To simplify the computation, the high energy end of the bremsstrahlung spectrum will be assumed square; i.e., it will be assumed that the number of quanta per unit energy interval is inversely proportional to the quantum energy (or, that $dN_\nu/dW \sim 1/h\nu$). Then, if F is the fractional part of W yielding quanta of energies between $h\nu_1$ (=3/4E) and $h\nu_2$ (=E), the number of quanta in this interval will be given by

$$N_\nu = FW \cdot \ln(\nu_2/\nu_1)/h(\nu_2 - \nu_1)$$

From Fig. 15 on p. 173 and Appendix I of Heitler[58] one obtains for aluminum that $\theta_{rad} = 1.50 \times 10^{-24} cm^2$/atom, and $N = 6.07 \times 10^{22}$ atoms/cm^3. From Fig. 14 on p. 170, loc. cit., one estimates that one-sixth of the bremsstrahlung energy will be distributed among quanta in the upper one-fourth of the energy interval, i.e., that F = 1/6. L (path length in aluminum) was experimentally determined to be 5,630 cm. Substituting these values into the equation above, one obtains $N_\nu \approx 98$. Or, in other words, had every particle assumed to have been a meson actually been a positron instead, one would have expected to have observed 98 events in which a positron lost more than three-fourths of its energy. Since no such events were seen,

the positron contamination must have contributed not more than the order of one percent to the total number of accepted particles in the meson beam.

It should be noted here that the radiation cross section θ_{rad}, used above, is actually for electrons. It applies equally well, however, to positrons. Positrons are subject, however, to annihilation in addition to radiation loss (see again Heitler[58], p. 230). Therefore, one would expect to have observed approximately 100 annihilation events also, had all the particles in the meson beam been positrons. These events would have been classed as stops. Only 20 stops were observed (Table I) and these were reasonably accounted for by corrections for meson scatters and stars hidden by the geometry.

APPENDIX III

EVALUATION OF GEOMETRICAL CORRECTIONS

A meson scattering event may be characterized by a scatter angle θ and azimuthal angle ϕ. θ is the usual angle between the meson directions before and after scattering. ϕ is measured with respect to rotation about the incoming meson direction taken as an axis. ϕ may also be used to describe the azimuthal orientation of a star configuration. The description of the configuration can be completed by assigning each fragment or "prong" its individual "scatter" angle θ.

The evaluation of the geometrical weighting factor for a given scattering or star event was carried out by imagining the event to be rotated about the ϕ axis, and observing the values of ϕ for which the configuration was obscured by the geometry. Since there is no reason to expect a preferred orientation with respect to rotation about the incoming meson direction, all values of ϕ were assumed to have equal probability. For simplicity, it was also assumed that the paths of particles involved in an event were straight (i.e., not curved by the magnetic field) and that the configuration, particularly with respect to star prongs, was unaffected by the changing paths in the aluminum brought about by the imagined rotation.

A track was considered to be hidden when it failed to traverse a minimum of approximately one-half inch of the illuminated region visible to the camera lenses. By idealizing the boundary conditions somewhat, it was possible to describe the orientation of an event with respect to the geometry of the aluminum plates and the illuminated region by the four parameters: θ, ϕ, β and γ. θ and ϕ have been defined above. The beam angle β is defined under "Experimental Procedure - Stereoscopic Projector." The parameter γ is an angle measured in a vertical plane. It depends upon the plate height at which an event takes place and upon the boundaries of the illuminated region. The trigonometric expression for ϕ in terms of θ, β, and γ was found to be rather complex and tedious to evaluate.

A simple "analog computer" was constructed to solve for the limiting values of ϕ much more simply. The following description of its operation may be understood by reference to Fig. 13. The axis of the hexagonal rod A represents the incoming meson and the knife edge (hidden in the photograph) of the bar B represents the outgoing scattered meson, or star fragment. The bar C defines the limits of observability set by the variable angle γ. The axis of rotation corresponding to the angular parameters θ, ϕ, β, and γ intersect in a common point coincident with the intersection of the axis of A and the knife edge of B. The protractors upon which θ, ϕ, β, and γ are measured are so labeled. Protractors β and γ are fixed to the base of the computer. Protractor θ is fastened to the hexagonal rod A, and the protractor ϕ is fixed to the block in which A rotates. This block itself is mounted so as to turn through the angle β.

When using the computer, θ and β are set to agree with the scatter angle and beam angle of the event being studied. For any one event the parameter γ has four values, corresponding to the four ways in which the upper and lower limits of illumination and the front and back sides of an aluminum plate can be combined. Once θ, β, and γ are set on the computer, the bar B is swung about the axis of A until it strikes the bar C. This position fixes one limiting value of ϕ. Three other values of ϕ are determined in a like manner to establish the range ($= \Delta\phi$) of ϕ in which the event is not hidden. One then divides the total range of ϕ ($= 360^{\circ}$) by $\Delta\phi$ to obtain the weighting factor for the event.

This weighting factor states the expected number of similar events if all could have been observed. It is applicable to scatters and one-prong stars. In the case of two-prong stars one proceeds in a like manner, determines the overlap in the ranges of ϕ for the two prongs, and obtains a similar weighting factor. One may also ascertain the proportion of the time the two-prong event would be expected to look like a one-prong star with the other prong being hidden. (The application of these weighting factors to the adjust-

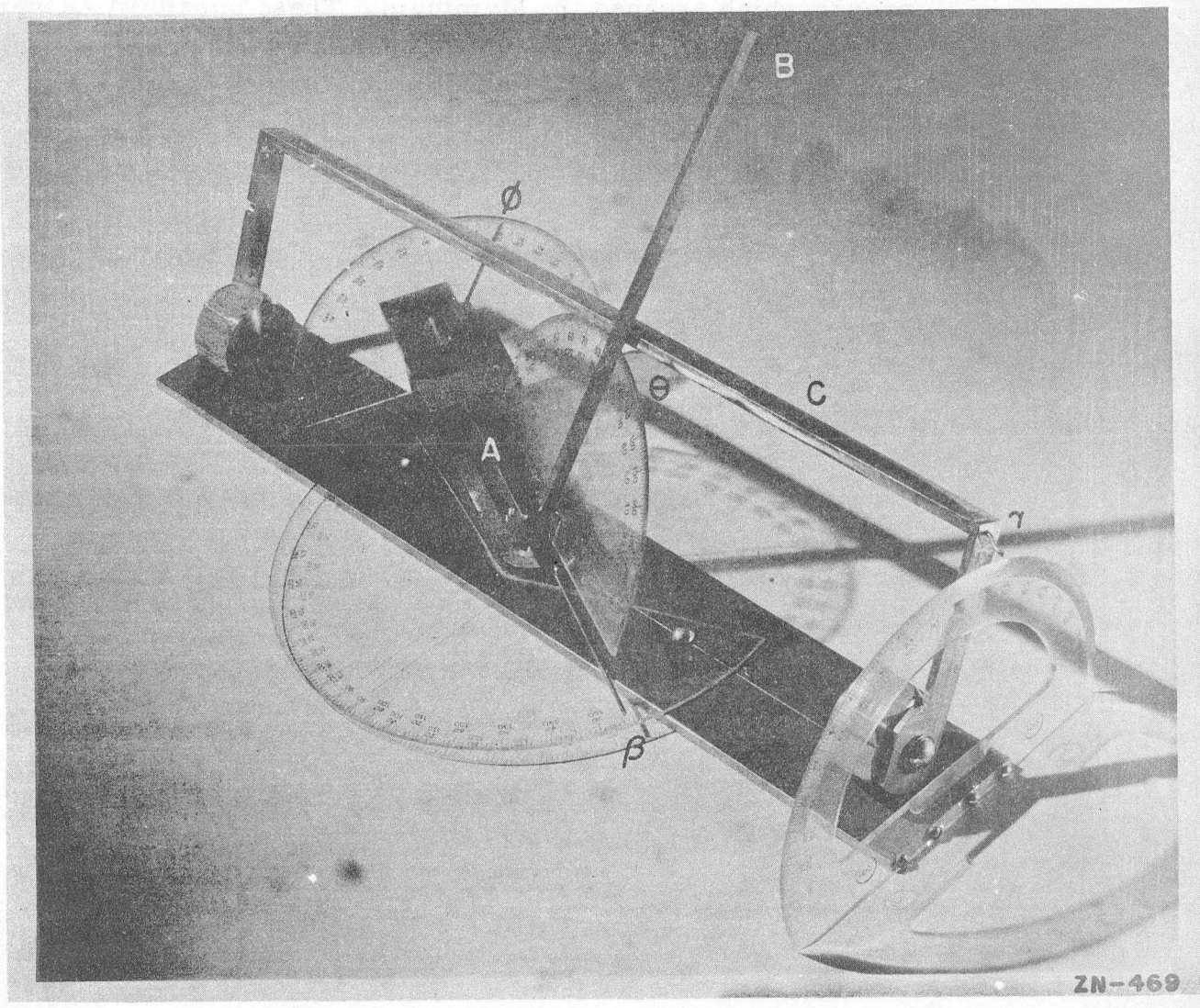

Fig. 13. - "Analog Computer"

This device aided in evaluating the geometrical corrections by determining the weighting factors to be applied to the several kinds of events.

ment of the numbers of events is outlined in Appendix IV). A remark regarding stars having more than two prongs - only two stars were found having more than two prongs, one a 3-prong star and the second a 4-prong star. Of course, some of the 1-prong and 2-prong stars (observed as such, at least) may actually have had more than two prongs which escaped the aluminum. These possibilities were considered to be so few in number (and so difficult to correct for) that they were ignored.

APPENDIX IV

ADJUSTMENT OF NUMBERS OF EVENTS

Let N^S = no. of actual scatters $\geqslant 30^o$, n^S = observed scatters $\geqslant 30^o$

N^0 = no. of real stops, n^0 = observed stops (real plus pseudo)

N^1 = no. of actual 1-prong stars, n^1 = observed 1-prong stars,

N^2 = no. of actual 2-prong stars, n^2 = observed 2-prong stars,

and

$N^S r^{S0}$ = no. of observed pseudo stops from actual scatters,

$N^1 r^{10}$ = no. of observed pseudo stops from actual 1-prong stars,

$N^2 r^{20}$ = no. of observed pseudo stops from actual 2-prong stars,

$N^2 r^{21}$ = no. of observed pseudo 1-prong stars from actual 2-prong stars.

Among the quantities defined above, the n's are the only ones obtained by direct observation. The N's and Nr's are only the most probable values, and their evaluation depends upon the introduction of certain assumptions stated below. The final quantities desired are the N's. The procedure for obtaining them follows.

The quantities which can be determined by use of the "analog computer" (see Appendix III, "Evaluation of Geometrical Corrections") are defined as follows:

f_i^{S0} = fraction of time the i^{th} observed scatter is expected to have appeared as an observed pseudo stop.

f_i^{10} = fraction of time the i^{th} observed 1-prong star is expected to have appeared as an observed pseudo stop.

f_i^{20} = fraction of time the i^{th} observed 2-prong star is expected to have appeared as an observed pseudo stop.

f_i^{21} = fraction of time the i^{th} observed 2-prong star is expected to have appeared as an observed pseudo 1-prong star.

Having defined the above quantities, one may write down the following relations:

$$N^S r^{S0} = \Sigma f_i^{S0}/(1 - f_i^{S0})$$

$$N^2 r^{20} = \Sigma f_i^{20}/(1 - f_i^{20} - f_i^{21})$$

$$N^2 r^{21} = \Sigma f_i^{21} / (1 - f_i^{20} - f_i^{21})$$

$$(N^1 + N^2 r^{21})\, r^{10} = \Sigma f_i^{10} / (1 - f_i^{10})$$

(The summations are carried over all the events in the categories for which the particular f_i's do not vanish.)

It is now possible to calculate the value of the N's providing one makes the following two assumptions: (1) $N^0 \equiv 0$, i.e., there were no real - as opposed to pseudo - stops; (2) $r^{10} \approx \bar{r}^{10}$, where

$$\bar{r}^{10} = \left[f_i^{10} / (1 - f_i^{10}) \right]_{\text{av.}}$$

One may now write:

$$N^S = \left[n^S + N^S r^{S0} \right]$$

$$N^0 = 0$$

$$N^1 = \left[n^1 + (N^1 + N^2 r^{21})\, r^{10} \right] - N^2 r^{21} (1 + \bar{r}^{10})$$

$$N^2 = n^2 + N^2 r^{20} + N^2 r^{21}$$

The results of these computations are displayed in Table I. The standard deviations have been determined from the number of events of each kind observed; i.e., $N^S \cdot \left[1 \pm (1/n^S)^{1/2} \right]$, $N^1 \cdot \left[1 \pm (1/n^1)^{1/2} \right]$, and $N^2 \cdot \left[1 \pm (1/n^2)^{1/2} \right]$.

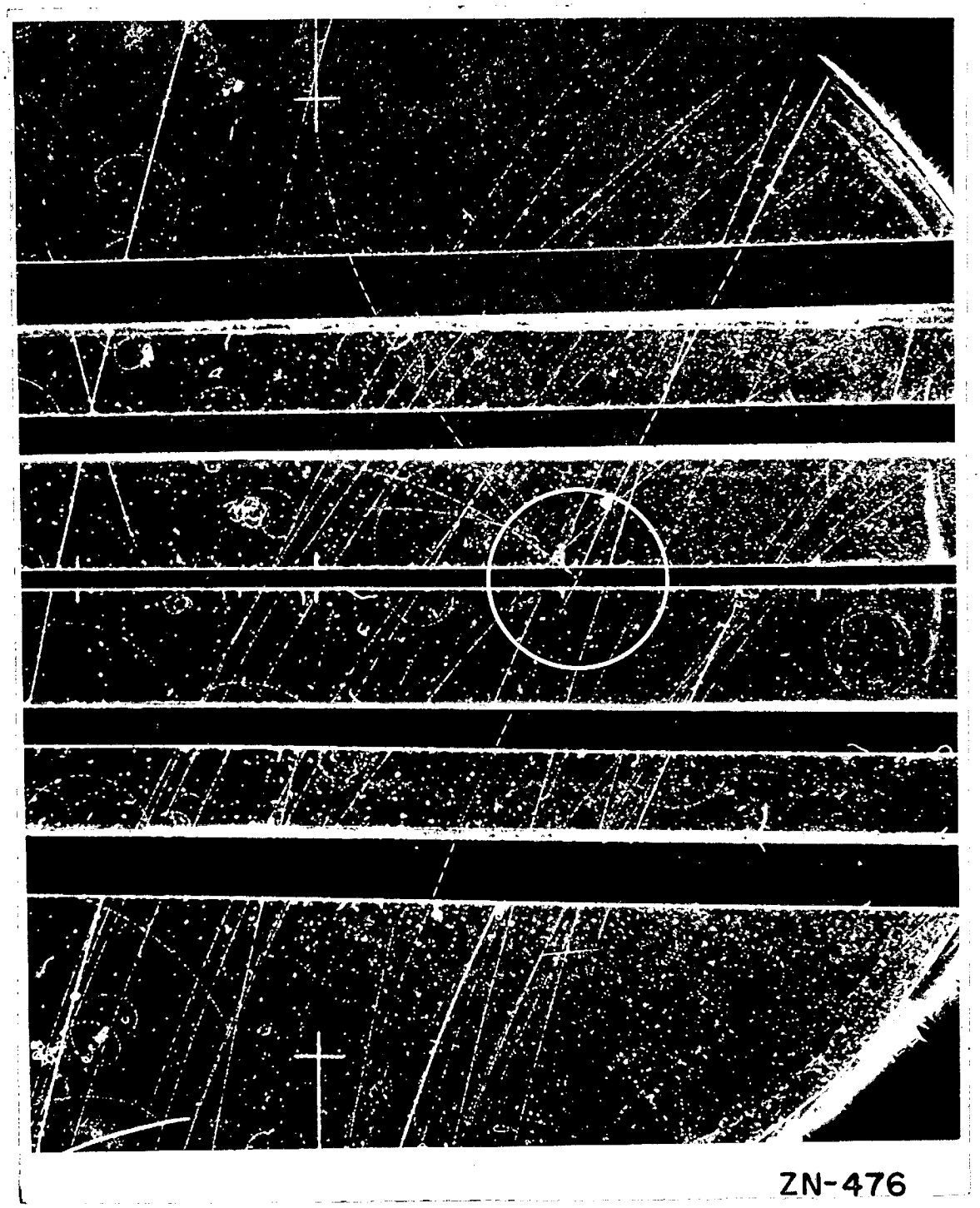

Fig. 14

An 88 Mev pion enters the third plate and, presumably, suffers a charge-exchange scatter. A 51 Mev proton is ejected at 6° to the forward direction; the neutral pion decays and causes a 70 Mev electron-positron pair to leave the plate at 75° to the forward direction. (The electron takes 28 Mev and the positron, 42 Mev.)

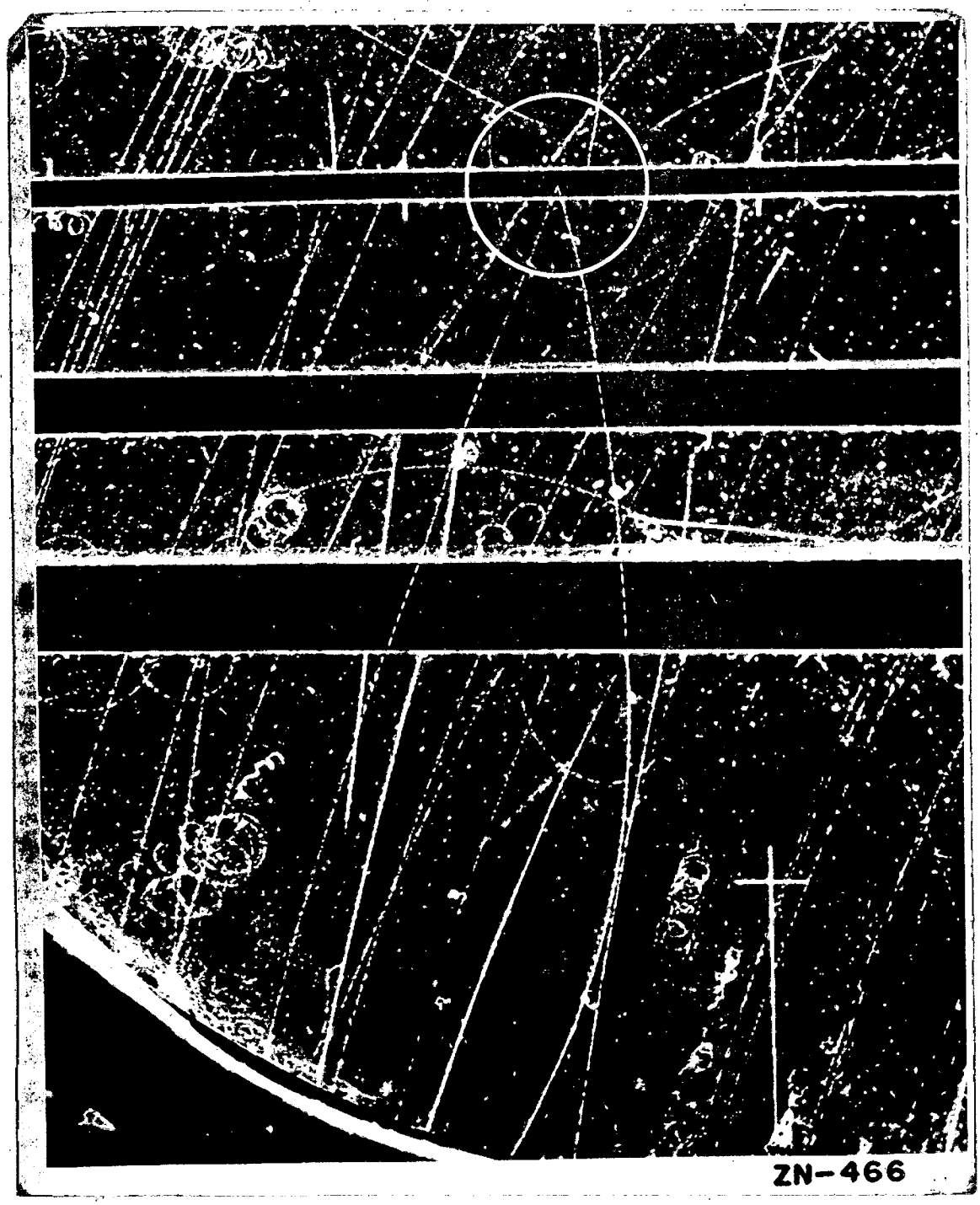

Fig. 15

A 67 Mev pion loses 5 Mev in traversing two aluminum plates, back scatters inelastically through 144° in the third plate, re-traverses the second and first plates, and leaves with an energy of 6 Mev. It lost about 40 Mev in the inelastic scattering process.

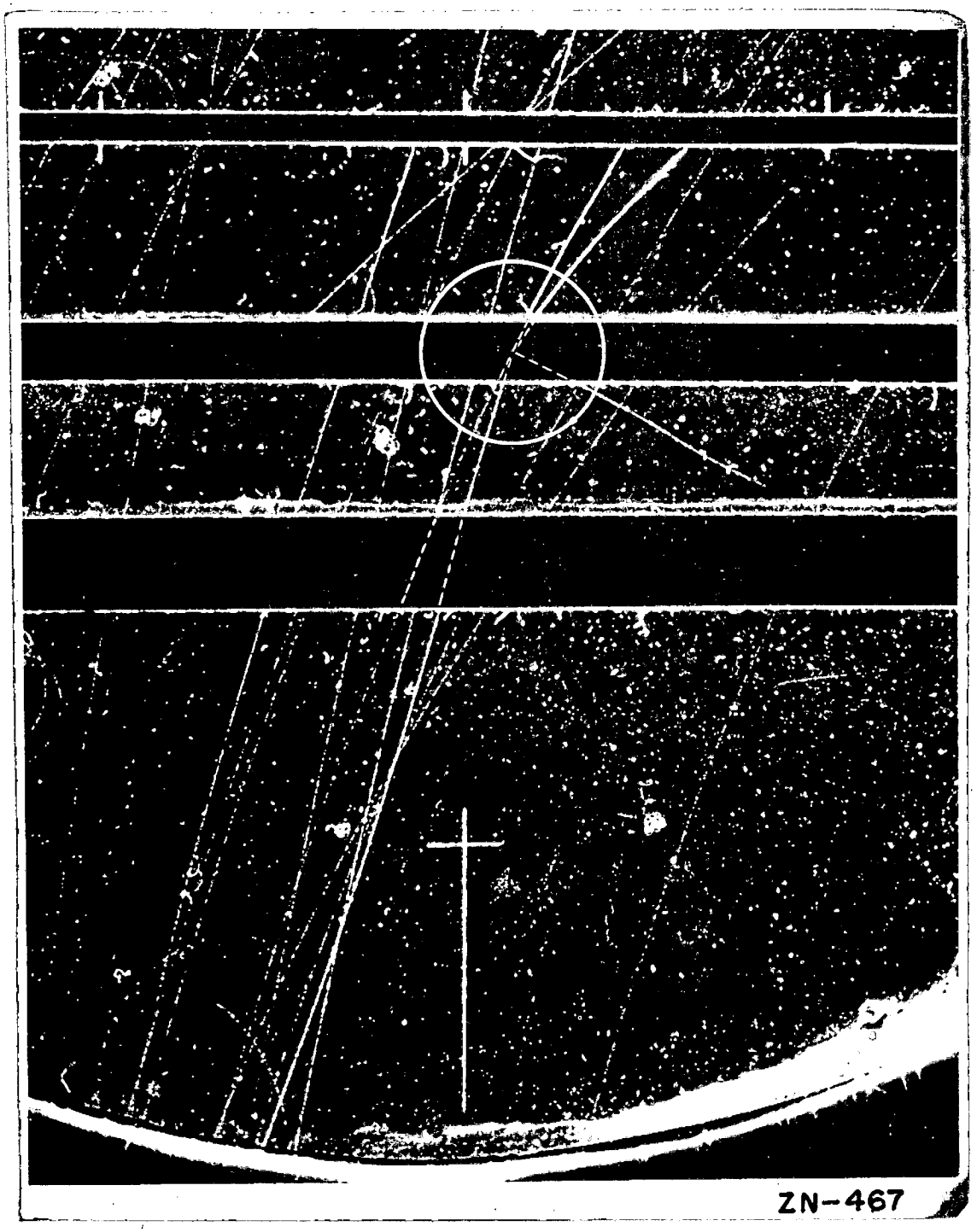

Fig. 16

A 59 Mev pion is absorbed by an aluminum nucleus, and four disintegration fragments are observed. The two heavy, forward fragments are probably protons of approximately 10 Mev each. The light, 90° fragment is a proton of $\geqslant 50$ Mev, and the backward fragment is a proton of approximately 50 Mev.

Fig. 17.

A 68 Mev pion scatters elastically through an angle of 50°.

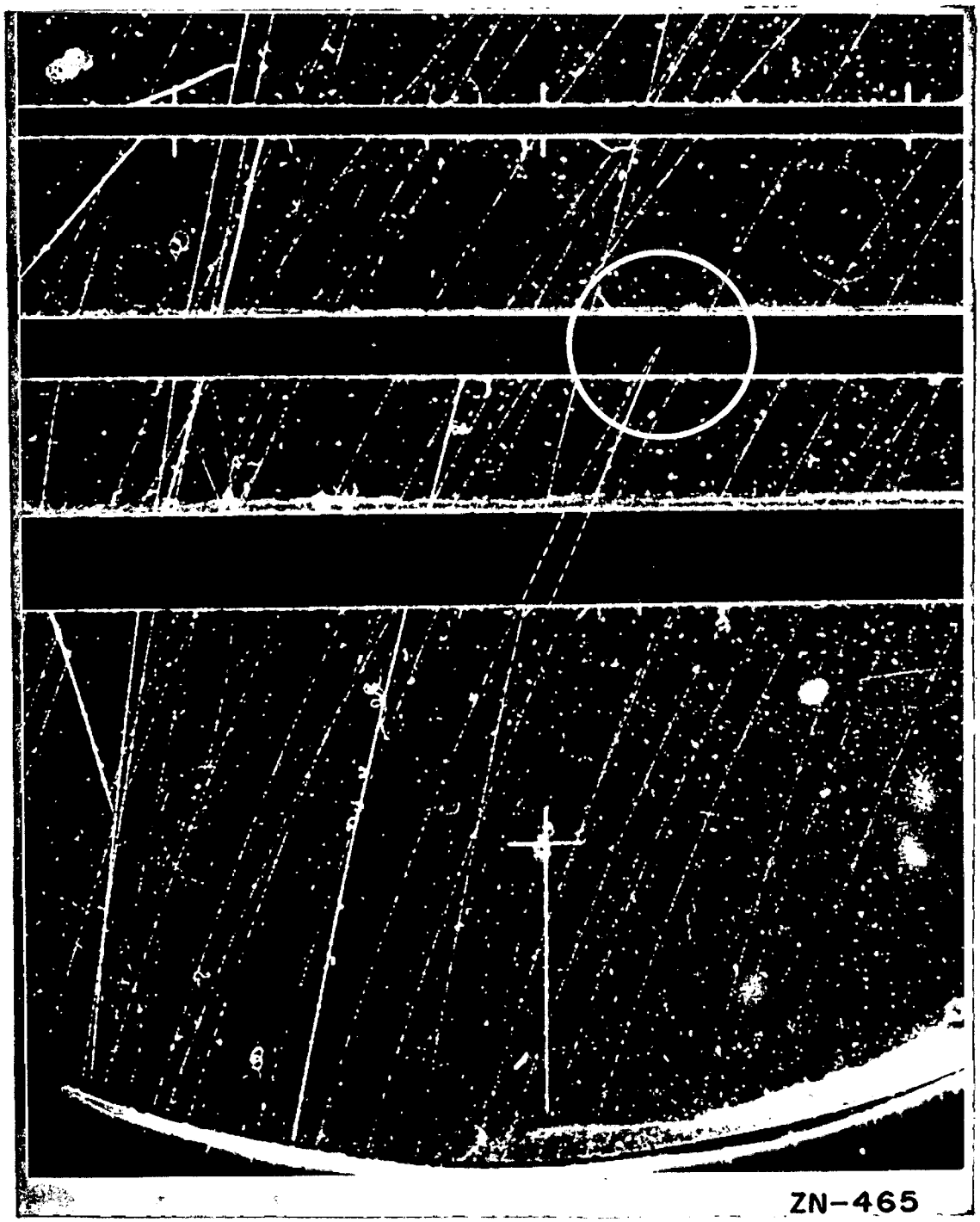

Fig. 18.

A 42 Mev pion enters the second aluminum plate. One disintegration fragment (probably a proton) is observed, leaving in a backward direction at an angle of 155° to the direction of the incoming meson.

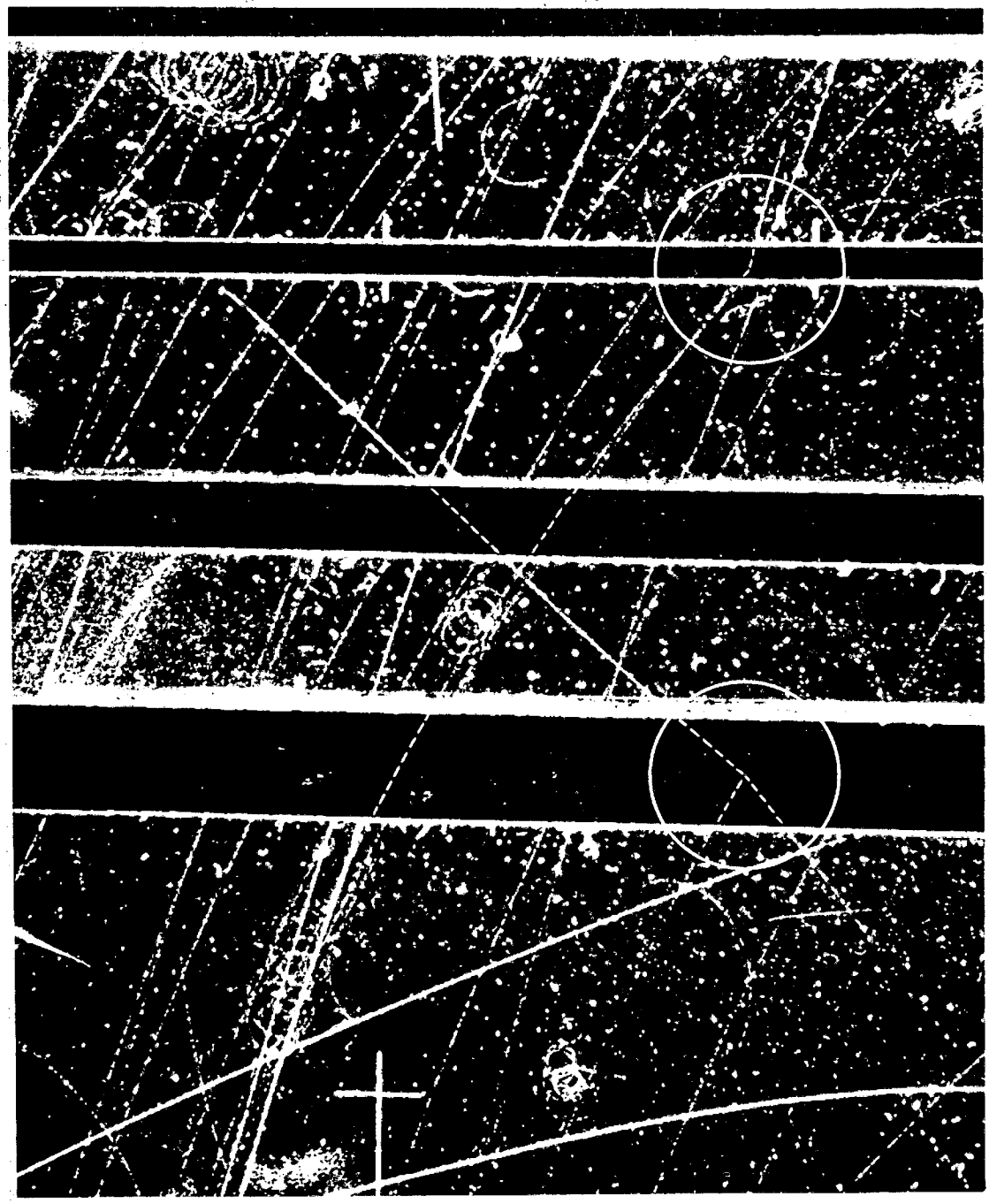

Fig. 19.

A 42 Mev pion enters a nucleus in the first plate and two fast protons, each of $\geq$ 50 Mev emerge in directions 164° to one another. A 21 Mev pion undergoes a forward scatter in the third plate. (This latter event was not included in the data because the pion energy was less than 25 Mev.)

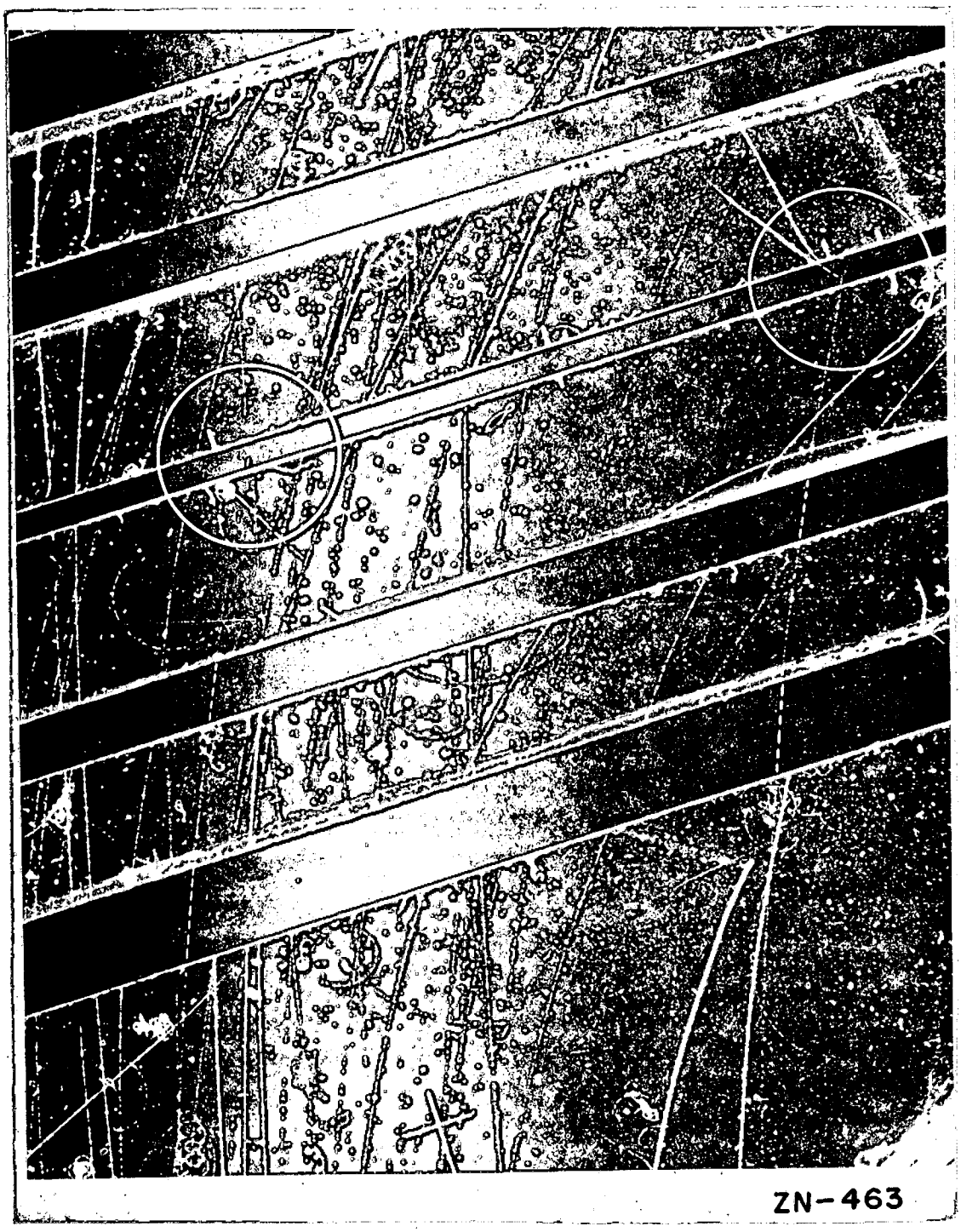

Fig. 20.

A 68 Mev pion enters the third plate (on the right) and one fragment - probably a proton of less than 20 Mev emerges. The second track is not associated with this event. A 96 Mev pion stops in the third plate (on the left).

REFERENCES

1. H. Yukawa, Proc. Phys. Math. Soc. Japan 17, 48 (1935).
2. C. D. Anderson and S. H. Neddermyer, Phys. Rev. 50, 263 (1936).
3. S. H. Neddermyer and C. D. Anderson, Phys. Rev. 51, 884 (1947), and Phys. Rev. 54, 88 (1938).
4. C. M. G. Lattes, H. Muirhead, G. P. S. Occhialini, and C. F. Powell, Nature (Lond.) 159, 694 (1947).
5. C. M. G. Lattes, G. P. S. Occhialini, and C. F. Powell, Nature (Lond.) 160, 453 (1947).
6. E. Gardner and C. M. G. Lattes, Science 107, 270 (1948).
7. F. Cartwright, C. Richman, M. Whitehead, and H. Wilcox, Phys. Rev. 78, 823 (1950), and Phys. Rev. 81, 652 (1951).
8. A. Langsdorf, Rev. Sci. Instr. 10, 91 (1939).
9. E. W. Cowan, Rev. Sci. Instr. 21, 991 (1950).
10. C. F. Nielsen, T. S. Needels, and O. H. Weddle, Rev. Sci. Instr. 22, 673 (1951).
11. R. P. Shutt, Rev. Sci. Instr. 22, 730 (1951).
12. G. D. Rochester and W. G. V. Rosser, Rep. Phys. Soc. Progr. Phys. 14, 227 (1951).
13. D. H. Perkins, Phil. Mag. 40, 601 (1949).
14. S. Tamor, Phys. Rev. 77, 412 (1950).
15. R. E. Marshak, Chapter on "Meson Physics," in Annual Review of Nuclear Science, Stanford, Calif., Annual Reviews, Inc., 1952, Vol. I.
16. G. Bernardini, E. T. Booth, and L. Lederman, Phys. Rev. 83, 1075 (1951), and Phys. Rev. 83, 1277 (1951).
17. G. Bernardini and F. Levy, Phys. Rev. 84, 610 (1951).
18. H. Bradner and B. Rankin, Phys. Rev. 87, 547 (1952).
19. B. Rankin and H. Bradner, Phys. Rev. 87, 553 (1952).
20. M. Camac, D. R. Corson, R. M. Littauer, A. M. Shapiro, A. Silverman, R. R. Wilson, and M. M. Woodward, Phys. Rev. 82, 745 (1951).
21. H. Byfield, J. Kessler, and L. M. Lederman, Phys. Rev. 86, 17 (1952).
22. C. Chedester, P. Isaacs, A. Sachs, and J. Steinberger, Phys. Rev. 82, 958 (1951).
23. R. L. Martin, H. L. Anderson, and G. Yodh, Phys. Rev. 85, 486 (1952).

24. R. L. Martin, Phys. Rev. 87, 1052 (1952).

25. R. Durbin, H. Loar, and J. Steinberger, Phys. Rev. 84, 581 (1951).

26. P. J. Isaacs, A. M. Sachs, and J. Steinberger, Phys. Rev. 85, 803 (1952).

27. H. L. Anderson, E. Ferni, E. A. Long, R. Martin, and D. E. Nagle, Phys. Rev. 85, 934 (1952).

28. H. L. Anderson, E. Fermi, E. A. Long, and D. E. Nagle, Phys. Rev. 85, 936 (1952).

29. H. L. Anderson, E. Fermi, D. E. Nagle, and G. B. Yodh, Phys. Rev. 86, 413 (1952), and Phys. Rev. 86, 793 (1952).

30. R. P. Shutt, E. C. Fowler, D. H. Miller, A. M. Thorndike, and W. B. Fowler, Phys. Rev. 84, 1247 (1951).

31. A. M. Thorndike, E. C. Fowler, W. B. Fowler, and R. P. Shutt, Phys. Rev. 85, 929 (1952).

32. R. L. Cool and O. Piccioni, Phys. Rev. 87, 531 (1952).

33. K. A. Brueckner, R. Serber, and K. M. Watson, Phys. Rev. 84, 258 (1951).

34. S. Fernbach, R. Serber, and T. B. Taylor, Phys. Rev. 75, 1352 (1959).

35. H. A. Bethe and R. R. Wilson, Phys. Rev. 83, 690 (1951).

36. M. H. Johnson, Phys. Rev. 83, 510 (1951).

37. J. Steinberger and A. S. Bishop, Phys. Rev. 86, 171 (1952).

38. A. G. Carlson, J. E. Hooper, and D. T. King, Phil. Mag. 41, 701 (1950).

39. J. J. Lord, J. Fainberg, D. M. Haskin, and M. Schein, Phys. Rev. 87, 538 (1952).

40. J. Steinberger to J. V. Lepore, private communication.

41. R. L. Mather, Phys. Rev. 84, 181 (1951).

42. C. Richman, M. Skinner, J. Merritt, and B. Youtz, Phys. Rev. 80, 900 (1950).

43. F. Crawford, K. Crowe, and L. Stevenson, Phys. Rev. 82, 97 (1951).

44. C. Richman and H. A. Wilcox, Phys. Rev. 78, 496 (1950).

45. W. F. Dudziak, Phys. Rev. 86, 602 (1952).

46. S. Leonard, private communication.

47. M. N. Whitehead and C. Richman, Phys. Rev. 83, 855 (1951).

48. W. M. Powell, Rev. Sci. Instr. 20, 403 (1949).

49. N. N. Das Gupta and S. K. Ghosh, Rev. Mod. Phys. 18, 225 (1946).

50. K. Brueckner, W. Hartsough, E. Hayward, and W. M. Powell, Phys. Rev. 75, 555 (1949).

51. J. F. Tracy, "Cloud Chamber Studies of the Stars in Oxygen," M. S. Thesis, Dept. of Electrical Engineering, Univ. of California, 1949, (UCRL-321).

52. J. H. Smith, Phys. Rev. 71, 32 (1947).

53. W. A. Aron, B. G. Hoffman, and F. C. Williams, "Range - Energy Curves," United States Atomic Energy Commission Report No. AECU-663, (UCRL-121), (1949).

54. O. Chamberlain, R. F. Mozley, J. Steinberger, and C. Wiegand, Phys. Rev. 79, 394 (1950).

55. M. Jakobson, A. Schulz, and J. Steinberger, Phys. Rev. 81, 894 (1951).

56. C. E. Wiegand, Phys. Rev. 83, 1085 (1951).

57. W. L. Kraushaar, Phys. Rev. 86, 513 (1952).

58. W. Heitler, The Quantum Theory of Radiation, 2nd. Ed. London, Oxford University Press, 1944.

59. W. F. Cartwright, Phys. Rev. 82, 460 (1951).

60. W. H. Barkas, Amer. J. Phys. 20, 5 (1952).

61. H. A. Bethe, Phys. Rev. 70, 821 (1946).

62. E. Amaldi and G. Fidecaro, Helv. Phys. Acta 23, 93 (1950).

63. E. P. George and J. Evans, Proc. Phys. Soc., Lond. 63A 1248 (1950).

64. B. Rossi and K. Greisen, Rev. Mod. Phys. 13, 263 (1941).